Title: **Optical Configuration and Straylight during Ground Testing**

CI-No:

Prepared by:	Dr. A. Frey, Dr. H. Hartmann	Date:	17.10.2003
Checked by:	Dr. E. Hoelzle		
Product Assurance:	R. Stritter		
Configuration Control:	A. von Ivady		
Project Management:	W. Rühe		

Issue	Date	Sheet	Description of Change	Release
1	22.11.02	1-29	First issue	
2	17.10.03	1-52	Second issue (completely revised)	

Table of contents

1 Summary

This technical note describes the selected optical configuration during ground testing. Basis was the action item (raised during the optical system working group meeting on 16 October 2002) initiating an investigation on retroreflecting elements to be placed on the closed cryocover. This note explains why the corner cubes have been replaced by concave mirrors. Closely related to that subject is the straylight to be expected during the ground test with a warm CVV ring.

A further basis for the work done here is the requirement on the optical background during ground testing. This requirement is evaluated in detail; it is shown that the associated accuracy of 25% (in terms of an absolute accuracy) can be considered as a goal, but not guaranteed. However, on a relative basis the optical power can be adjusted to a broad range of optical background desired by the scientists.

The technical solution found has the properties

- ground testing does not induce intolerable straylight for the experiments
- thermal/straylight problems of a black cryocover in orbit are avoided
- contamination hazard is reduced.

The results for scattered light show values of 9% (with telescope = 100 %) for SPIRE while the values found for PACS are near 5%. This difference is due to the position of the SPIRE thermal filter 1 near to the SPIRE entrance, the corresponding PACS filter is positioned far away from the entrance.

In addition, a review of the scattering functions had revealed that the specific one for the cryocover mirrors (used in issue 1, also used up to the quarterly progress meeting July 2003) may have been too optimistic. Therefore the pessimistic one of the telescope mirrors is now applied instead leading to increased irradiances. Also an increase of the gap width below the CVV and a temperature change of the thermal shield 2 baffle contribute to an increase in irradiance.

The diffraction calculations show satisfactory values for most cases. Exceptions are

- long wavelengths of SPIRE
- the case of experiment internal misalignment with a direct view from the detectors onto strongly irradiated edges.

The straylight results are given (as usual) in % with 100% = telescope irradiation (70 K, total ε=0.03). If the telescope will have a substantially lower emissivity (present tendency), then these relative values will increase accordingly.

2 Configuration

2.1 General Concept

The general concept consists of elements (mirrors, flat disks) in the closed cooled cryocover within the direct field of view of the experiments. The temperature of those cooled elements (in connection with their emissivity) shall induce a background radiation comparable to that expected from the telescope in orbit.

Basis for that part of the investigations which have started in October 2002 was the proposal from SPIRE for corner cubes as retroreflecting elements on the cryocover. The idea is that the SPIRE and PACS should 'see' themselves during the ground test, i.e. see a known cold background. In addition, SPIRE and PACS should see the corner cubes cooled to such an extent that the expected radiation of the telescope is simulated.

There are two tasks to be accomplished

- simulation of the desired background (as from the telescope in orbit)
- fulfilment of the concept that the experiments see ‘themselves’

It will not be easy to implement corner cubes on the cryocover surface (mass, smallest allowed aperture dimension, etc.). Moreover the scattering function of an array of corner cubes will be appreciable (disadvantageous w.r.t. the problem of the warm CVV ring). Therefore alternatives were searched. The alternative proposed here is that both SPIRE and PACS view onto individually adapted concave mirrors on the cryocover.

By proper selection of the emissivity of these mirrors the desired background can be created. Roughly the cryocover mirror emissivity should be twice that of a single telescope mirror. Since the emissivity is difficult to reach a priori in the far infrared, a sample program has to be initiated with

- special surface treatment of several mirror samples
- measurement of the emissivity in the far infrared at one of the laboratories cooperating with the project Herschel
- choice of the best surface treatment.

By proper selection of their curvature the mirrors are suitable for the purpose that SPIRE and PACS 'see' themselves. The configuration is shown in figure 2.1-1.

Figure 2.1-1: Configuration with two concave mirrors on the closed cryocover, backward trace of rays from the detectors onto the cyryocover

The advantages of those concave mirrors (compared to the corner cubes) are

- smaller scattering function
- more simple mechanical bodies.

The apparent advantage of corner cubes (exact retroreflection in direction) is not important, since the retroreflection by corner cubes is accompanied by a lateral shift, this shift is important in a non-collimated situation. So both the corner cubes and the concave mirrrors do not achieve that a specific detector pixel is imaged back onto itself, instead the detector pixel is imaged onto a spot somewhere in the same experiment.

The positions of the spots of the backward trace onto the cryocover mirrors can be seen more clearly in figure 2.1-2 where the telescope axis is perpendicular to the picture.

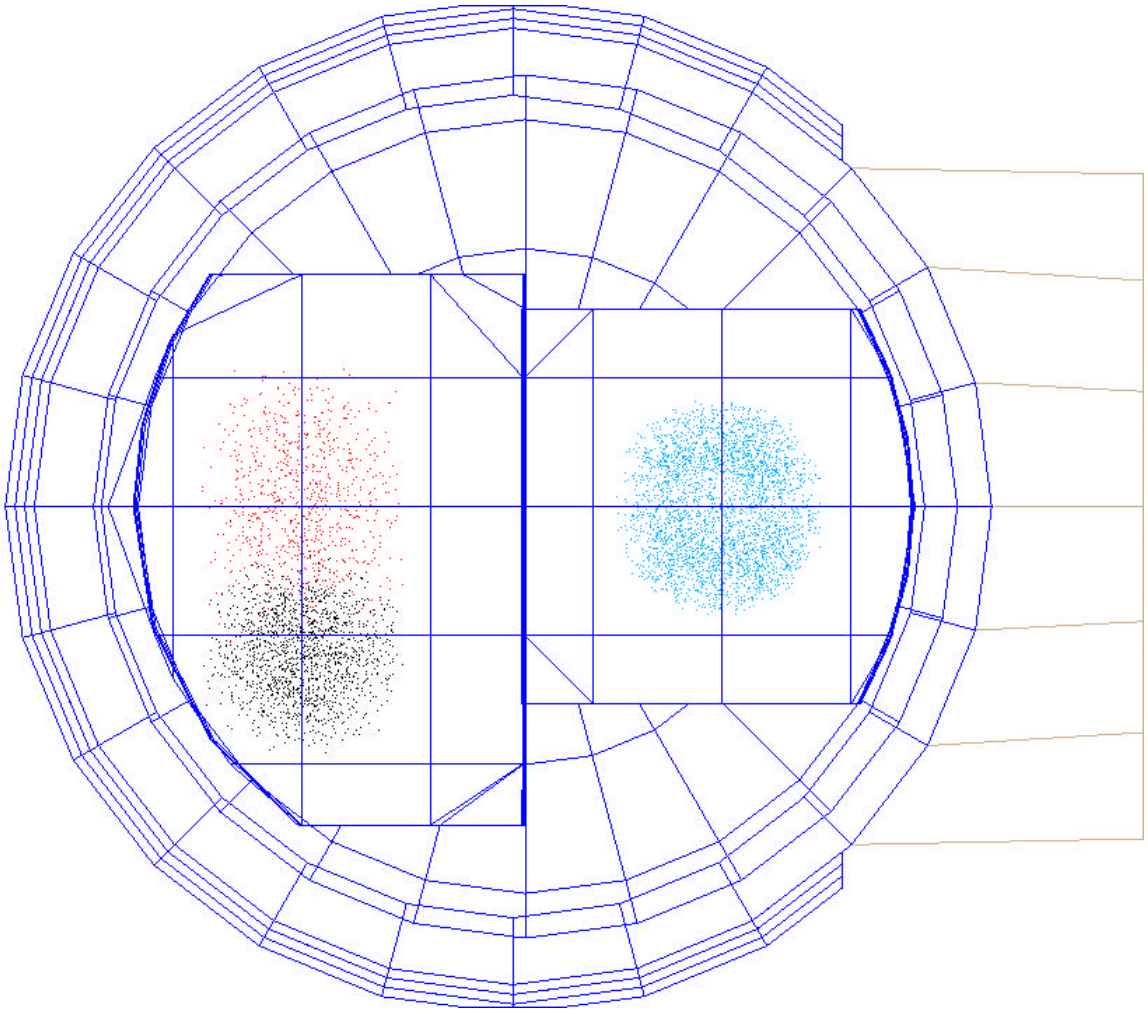

Figure 2.1-2: Spots of the backward trace of figure 1 on the cryocover mirrors;
left: mirror for SPIRE
right: mirror for PACS (spots for the zero value of the chopper angle)

The concave mirrors have been given fairly large margins around the spots, the mirrors are limited by

- the round circle of the cryocover itself
- the straight lines within the area of the cryocover.

One can see that there are comfortable margins at the straight limits of the mirrors while the circular limit of the cryocover is not able to deliver a comparable margin for SPIRE (this limitation exists for any kind of object on the cryocover, not only for these mirrors).

The spots in the backward trace have been gained mainly by the ASAP models as used up to now. In addition, the SPIRE spectrometer path (not contained in the present ASAP model) has been simulated by using

- data for the spectrometer field in system focal surface found in SPIRE-RAL-NOT-000581
- the assumption that the spectrometer beam fills the telescope secondary mirror.

Thus the ASAP spectrometer path exists only from the system focal surface (up to M2). The corresponding spots on the cryocover mirror are those placed with an offset below that for the photometer.

The discussion on the optical working group meeting on 16 October 2002 resulted in the statement that HIFI did no longer reject edges on the cryocover surface (otherwise both corner cubes and mirror edges were not allowed). Thus the mirrors for SPIRE and PACS are extended up to the center of the cryocover where the beam for HIFI is found. There a single edge is present.

The chopping strategies to be considered for PACS and SPIRE during ground testing are quite different

- the calibration radiation of SPIRE is fed in through a hole in the very center of the SPIRE chopper, therefore there is no chopping action needed for calibration purposes
- the calibration radiation of PACS is fed in along two paths only accessible by chopper action, therefore the chopping action is needed for calibration purposes, the detector view crosses the cryocover path during transition between both calibrations positions.

For that reason we leave the beam for SPIRE in the non-chopped position whereas for PACS also a position with chopper action is added. This is shown in figure 2.1-3 where the PACS chopper has been tilted by an angle of 2.9 degrees (angle for the chopper itself); no chopping tilt was introduced for SPIRE. The chopped positions on the PACS cryocover mirror do not impose any difficulty.

The data for the spectrometer field in system focal surface found in SPIRE-RAL-NOT-000581 probably contains an extension including the chopped positions, i.e. it is overestimated, the non-chopped field is smaller.

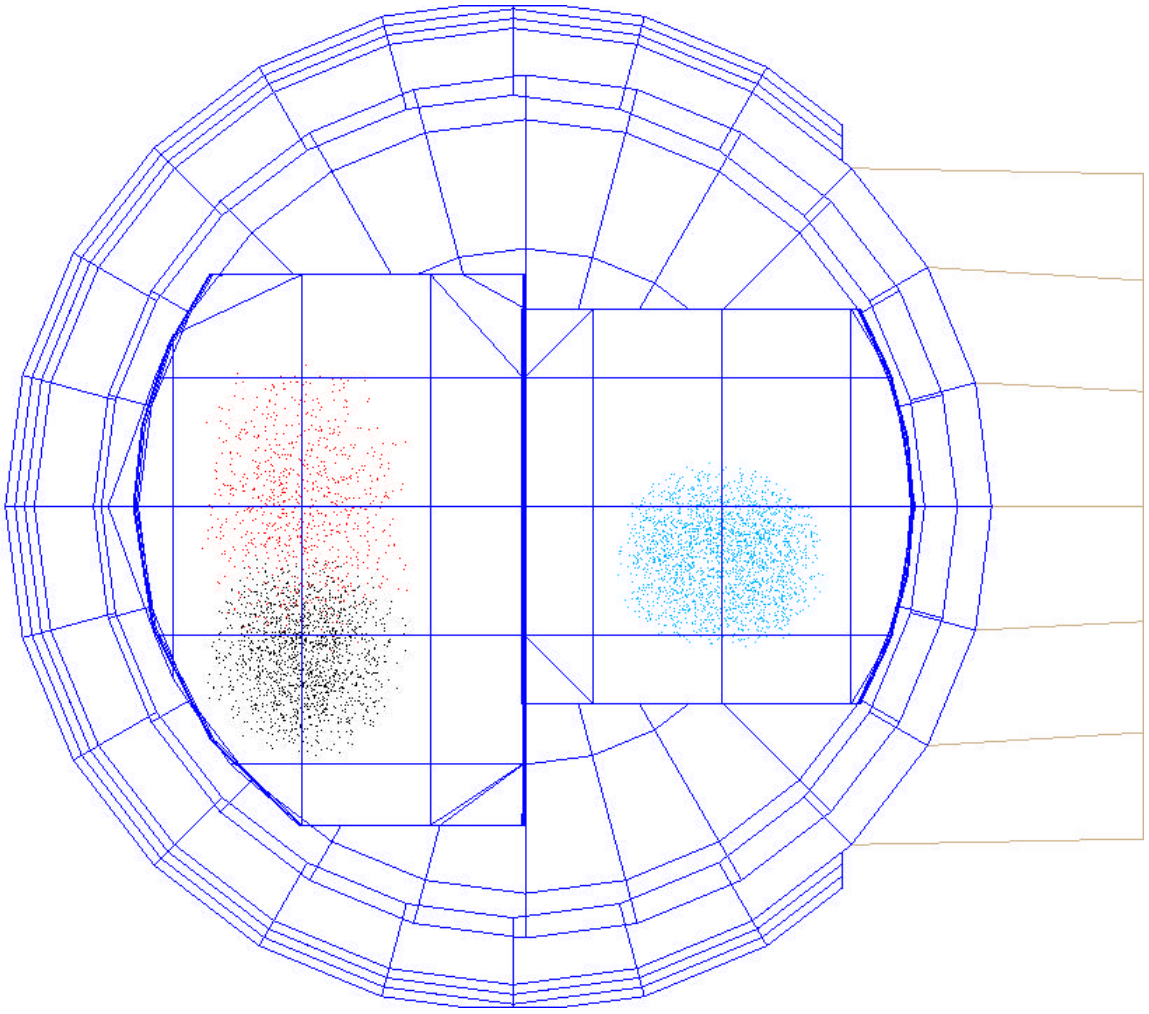

Figure 2.1-3: Spots on the cryocover mirrors;
left: mirror for SPIRE
right: mirror for PACS (spots have an offset due to the chopper angle of 2.9 degrees).

2.2 Do the experiments ‘see’ themselves?

It was stated that the experiment detectors should not have a view onto surfaces (during ground testing) which may receive strong off-axis radiation. So surfaces within the experiments were chosen as targets onto which the experiment detectors may have a direct view.

This ‘view criterion’ is stated as:

- the SPIRE detector should view onto thermal filter 1
- the PACS detector should view onto the opening between the rearview (calibration) mirrors.

In the following discussion we always place the 'eye' of the experiment onto its detector and 'see' backwards towards the cryocover (as in figure 2.1-1). The beams reflected by the cryocover mirrors, then, is what the detectors 'see' in reflection, this reflection is a forward direction, i.e. that from cryocover to experiment.

The reflections into the experiments require most attention. There is only a single degree of freedom available for the axial positioning of the reflected image planes and pupil planes, i.e. the curvature of the cryocover mirror, since the position is fixed. Therefore either the reflected image plane or the reflected pupil plane can be positioned axially at will, not both.

We encounter two main strategies

- a radius of curvature around 440 mm for the cryocover mirror places the reflected image plane onto itself, the reflected pupil plane is above the experiments
- a radius of curvature around 600 mm for the cryocover mirror places the reflected pupil plane a little bit above the telescope system focal surface (i.e. near to the experiment entrance), the reflected image plane is shifted into the experiment.

The radii of curvatures were optimized with the ‘view criterion’ in mind. In general they are somewhat shorter than presented in the issue 1 of this TN (i.e. mostly follow the first strategy).

Compared to the first issue of this technical note, there was a considerable change in the ASAP model for PACS

- there is a new data basis for the modeling of all mirrors, i.e. an Excel sheet with mirror data; the ASAP commands for the mirrors have been set up by Astrium; the diffrerence to the earlier mirror geometry mainly affects the mirror limitations (not the curvatures)
- all calibration mirrors are modeled now
- the entrance opening is modeled now.

One of the consequences of the details of the new PACS model is a reduction of the margin near the opening for PACS. The reflected beam patterns on the entrance opening (X=252.5) are shown in figures 2.2-1 and 2.2-2. A side view of a forward trace from cryocover mirror up to TROG1 is shown in figure 2.2-3.

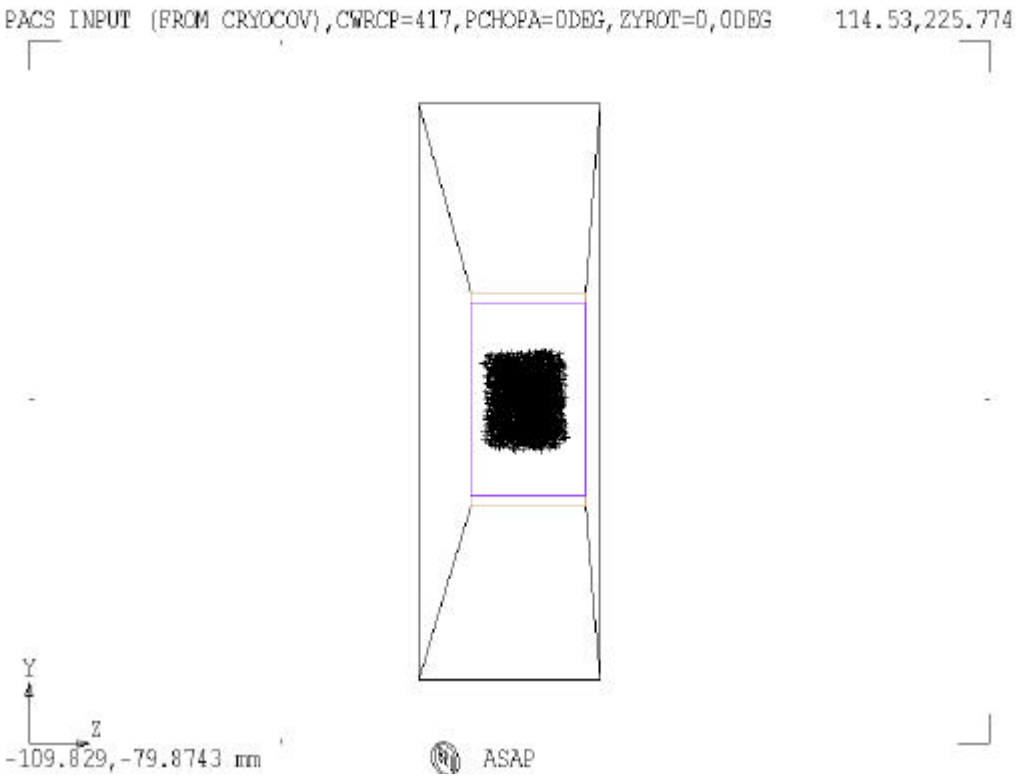

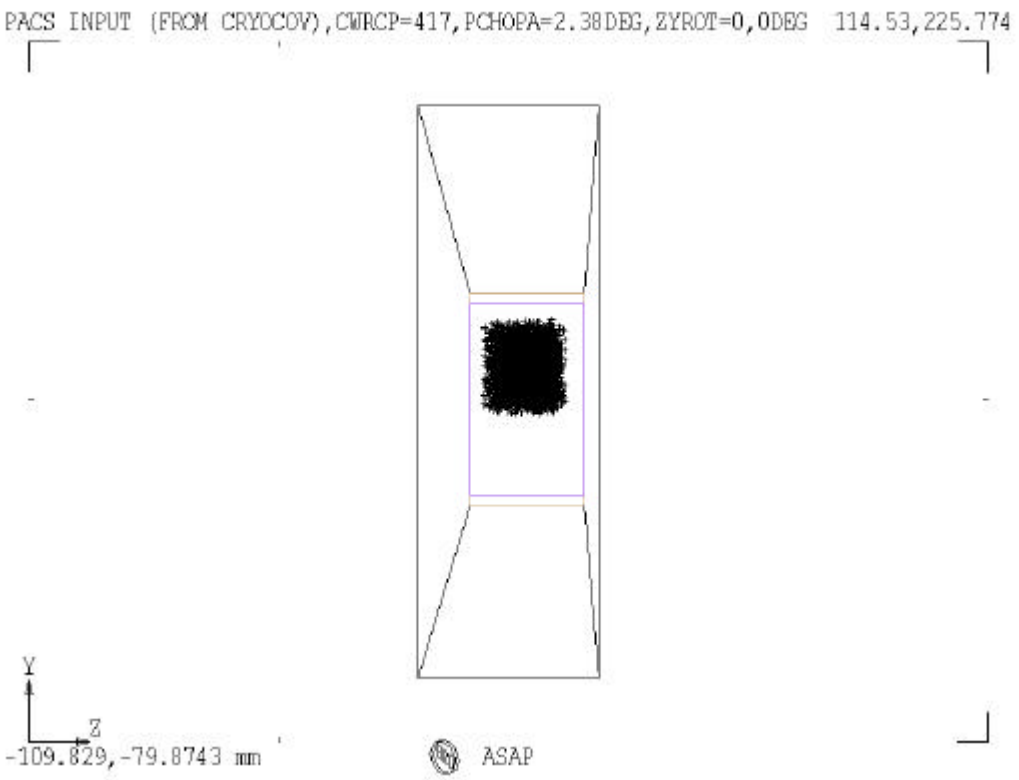

Figures 2.2-1 (above) and 2.2-2 (below): Spots of the beam reflected by the PACS cyrocover mirror on PACS input opening (X=267 above TROG1); chopper angle is 0 degrees (above), 2.38 degrees (below).

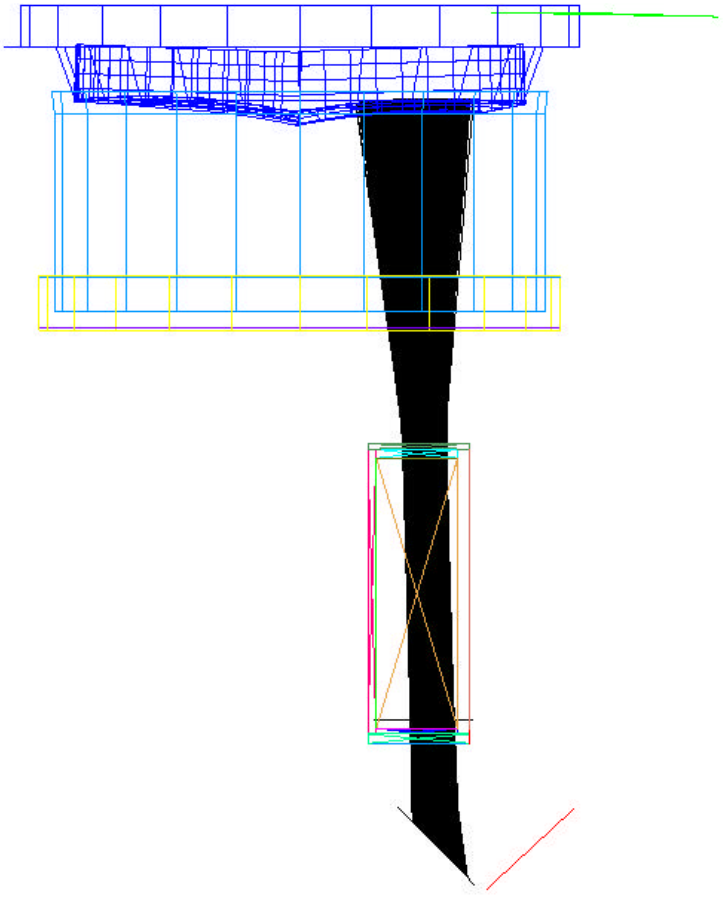

Figure 2.2-3: Rays of the backward trace (of figure 2.1-1) restarted at the PACS cryocover mirror (in forward direction) up to TROG1 of PACS, all these rays pass the PACS input and reach TROG1.

The placement of the cryocover mirror for SPIRE is determined by the desire to send back the photometer field through the larger part of the FP-UNIT-baffle (not through the slim part of the spectrometer). Therefore the reference point of the SPIRE cryocover mirror is in the center of the photometer field of view, the mirror normal at this reference point is made parallel to the chief ray of the photometer. The spectrometer field, then, is sent back with a larger oblique angle. In order to reduce that oblique angle, we introduce a reduction of the curvature of the SPIRE cryocover mirror along the Y-coordinate, i.e. the SPIRE cryocover mirror is toric. Then the reflected spectrometer beam can be placed on the center of thermal filter 1. This technique works because the beams overlap only to a small degree on the cryocover mirror. The corresponding spots and the traces are shown in figures 2.2-4 and 2.2-5.

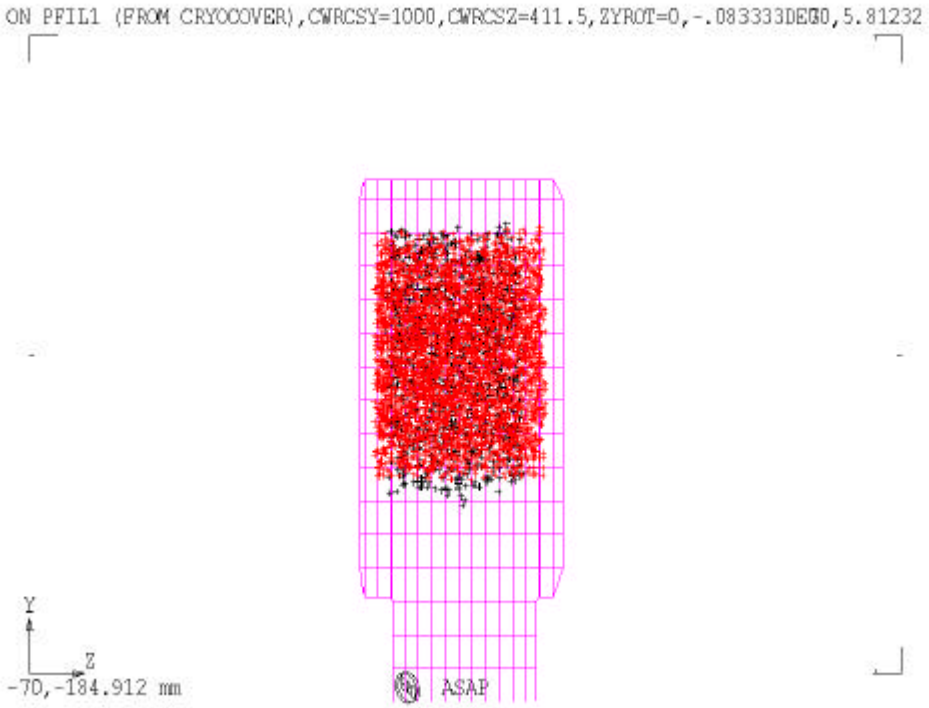

Figure 2.2-4: Spots of the beam reflected by the SPIRE cyrocover mirror on thermal filter 1 (black spots are spectrometer rays)

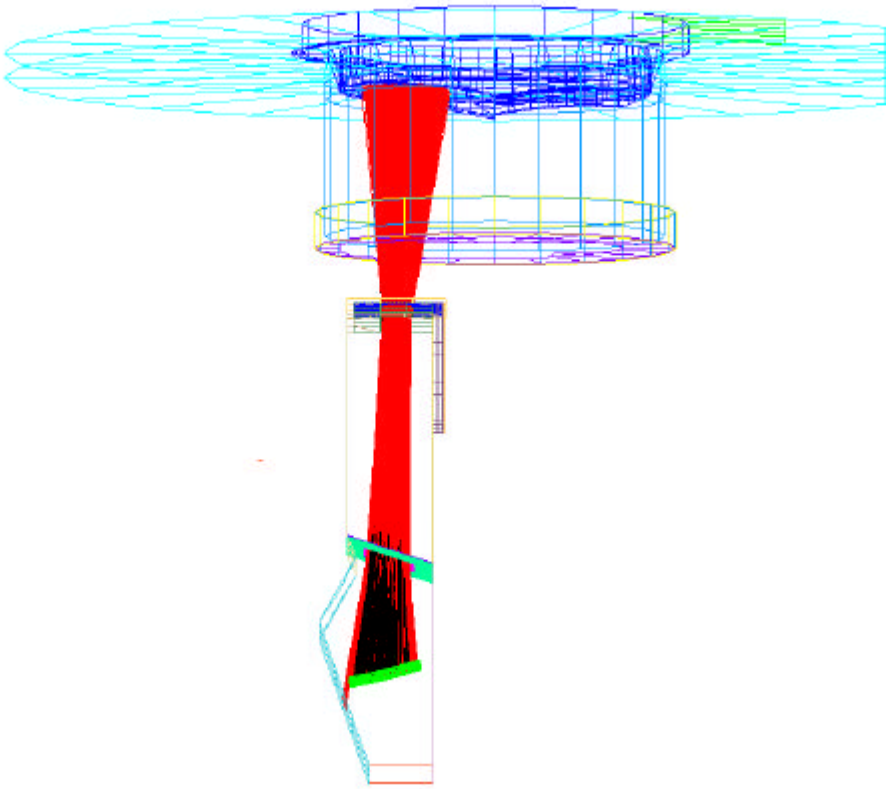

Figure 2.2-5: Rays of the backward trace (of figure 2.1-1) restarted at the SPIRE cryocover mirror up to M3 of SPIRE, all these rays also pass thermal filter 1 up to M3.

The preceeding pictures present the ideal geometry, i.e. without any misalignment. In reality, misalignment has to be taken into account. Two version of the cryocover mechanics are treated here

- a special alignment jig (ground support equipment) is used for adjusting the cryocover to a symmetrical centered position and orientation.
- manufacturing accuracy assumed for the mechanical components of the cryocover

The following table shows the accuracies available with both options.

Table 2.2-1: Alignment accuracies achievable for the beam on the experiment openings

	error	beam shift (mm)
cryocover/mirror assembly equipped with alignment jigs (GSE, total shift):	0.70 mm	1.40
experiment internal misalignment (only guess)	1.0 mm	2.00
interface CVV-cyrocover versus OBA (position)	0.2 mm	0.40
interface CVV-cyrocover versus OBA (angle)	0.33 arcmin	0.08
instrument versus OBA	1.0 mm	2.00
linear sum		5.88
rss- sum		3.18

	error	beam shift (mm)
cryocover/mirror assembly without alignment jigs (position)	1.25 mm	2.50
cryocover/mirror assembly without alignment jigs (angle)	15 arcmin	3.49
experiment internal misalignment (only guess)	1.0 mm	2.00
interface CVV-cyrocover versus OBA (position)	0.2 mm	0.40
interface CVV-cyrocover versus OBA (angle)	0.33 arcmin	0.08
instrument versus OBA	1.0 mm	2.00
linear sum		10.47
rss- sum		5.16

The available margins are of the order of several millimeters (both for PACS and SPIRE). Thus a realistic chance for the fulfilment of the ‘view criterion’ stated above is given only with the presence of alignment jigs (for misalignments along Z-direction). If it is not fulfilled for unfavourable combinations of the individual errors listed above:

- the SPIRE detector, then, views onto thermal filter 1 and a small part of its mechanical rim (still within the SPIRE input compartment)
- the PACS detector, then, views onto the opening between the rearview (calibration) mirrors and a small part of the nearby black mechanical stop (on PACS itself).

It will be shown in chapter 4 that these small violations of the view criterion do not have a large impact on the straylight, thus the deletion of the alignment jigs is an acceptable option.

2.3 Configurational Data

The present optical configuration is characterized by the chief rays of SPIRE and PACS, they are listed in table 2.3-1 by coordinates of several points

- XYZ of a selected cryocover mirror reference point
- XYZ in the telescope system focal surface
- XYZ of the mirror center of curvatures.

The surface normals of the cryocover mirrors at those reference points are parallel to the chief rays mentioned. The data in table 2.3-1 are cold operating data, the corresponding warm data given to the manufacturers differ (not only because of the transition warm-cold, but also due to a correction allowing for pressure deformation).

Table 2.3-1: Data for the cryocover mirrors (operational state)

SPIRE mirror (toric)	X	Y	Z
mirror reference point on closed cryocover	622.760	0	-76.457
field center in system focal surface	226.609	0	-90.116
radius of curvature (along Y and Z)		996.04	409.87
center of Y-curvature	-372.637		-112.226
center of Z-curvature	213.155		-91.176
PACS mirror (spherical)	X	Y	Z
mirror reference point on closed cryocover	622.761	0	67.242
field center in system focal surface	221.114	0	79.420
radius of curvature (along Y and Z)		415.349	415.349
center of curvature	207.603		79.830

The preparations for the manufacturing capabilities for the toric mirror have revealed that the exact toric figure is not easily achievable. Instead a slight deviation (proprietary information) leads to easier manufacturing. This deviation induces a slight enlargement of the spots in Y-direction in figure 2.2-4, which is acceptable.

2.4 Design Options

Several design options exist which are summarized in the table below. Present discussions aim at the choice of option no. 2 due to cost reasons. The consequence will be a small alignment penalty (and consequently a small straylight penalty) to be paid for that cost saving (compared to option 1).

Options 3 to 5 are mentioned only since they have been in discussion, their severe disadvantages (in our opinion) have to lead to rejection:

- option 3 will have no special (mirror) surface treatment, so a background prediction is impossible, this leads to an exclusion of this option
- options 4 and 5 will have excessive straylight, so can be excluded as acceptable options.

The purpose of the following chapters 3 and 4 is to present quantitative data and results underlining these qualitative statements.

Cryocover Designs in discussion

design option	properties
1) • equipped with curved mirrors • dedicated alignment during assembly with the aid of alignment jigs (dedicated GSE), • special mirror surface treatment	• good alignment accuracy, detectors 'see' via reflection only (as desired) ♦ opening of input stop (PACS) ♦ thermal filter 1 (SPIRE) • tolerable straylight • good chance to reach desired emissivity
2) • equipped with curved mirrors • alignment accuracy according to manufacturing accuracy • special mirror surface treatment	• fairly good alignment accuracy, detectors 'see' via reflection only ♦ opening and small part of input stop (PACS) ♦ thermal filter 1 and small part of its rim (SPIRE) • moderate straylight increase compared to case 1) • good chance to reach desired emissivity
3) • equipped with curved mirrors • alignment accuracy according to manufacturing accuracy • no special mirror surface treatment	• rejected mainly due to low chance to reach desired emissivity • no good alignment accuracy • detectors 'see' only (in reflection) ♦ opening and rim of input stop(PACS) ♦ thermal filter 1 and its rim (SPIRE) • straylight increase compared to cases 1) and 2)
4) equipped with simple black surface	rejected due to • straylight in excess of desired telescope background (considerable excess if telescope mirrors indeed have low emissivity), therefore: • background not adjustable
5) equipped with simple reflecting surface	rejected due to • not accepted by scientists • straylight in excess of desired telescope background (estimate, no calculation) considerable excess if telescope mirrors indeed have low emissivity, therefore: • background not adjustable

3 Establishment of the Thermal Background

The thermal/radiometric requirements on the cryocover consists of the establishment of a background similar to that of the telescope objects in orbit (including the expected straylight contribution).

In detail:
„It shall be possible to provide an optical representative environment for the instrumental focal plane within the cryostat in cold condition on ground, such as to allow functional and performance verification of these units after system integration and test. This environment shall represent the optical power coming from the telescope in orbit, i. e. 70K @ 4% emissivity, to an accuracy of 25%, in the six wavelength bands of SPIRE and PACS over the [80-670 µm] range while taking into account all system requirement such as straylight.
EQM and PFM might use different concepts.“
(EPLM AIV & Satellite AIT Requirements, AIAI-52).

It is expected that the desired emissivity ε will be substantially smaller due to the recent measurements of the telescope emissivity ε, which turns out to be smaller than predicted. It is planned to assign a value to the desired emissivity by information exchange between all relevant parties shortly before manufacturing.

The optical power P is determined by the following relation

$$P = L(BB(T)) * \varepsilon * S(Y,Z,\beta,\gamma) * A * \Omega + Str$$

with

L(BB(T))	radiance of a blackbody of temperature T
ε	Emissivity
$S(Y,Z,\beta,\gamma)$	sensitivity of the instrument as function of position (Y and Z) and angles (β and γ) at the X-coordinate of the cryocover mirrors
A	area up to cutoff of function $S(Y,Z,\beta,\gamma)$
Ω	solid angle up to cutoff of function $S(Y,Z,\beta,\gamma)$
Str	straylight to be expected during the test

The required accuracy of 25%, then, can only be accomplished, if smaller individual errors for each factor in the equation mentioned above can be allocated. The following lines give estimates for those errors.

When supplying the required power, the only conceivable way is to overfill the area and solid angle of the instruments by offering a larger radiating surface with known radiance, the instruments cut out their corrsponding area and solid angle with their sensitivity $S(Y,Z,\beta,\gamma)$. This sensitivity is not constant over Y, Z, β, and γ, also the radiance of the radiating surface is not exactly constant. Both irregularities create a mismatch between the required power and the delivered one, we tentatively attribute 20% for the corresponding error (this is only a guess).

The radiance L(BB(T)) can be adjusted by changing the (measured) temperature T of the cryocover, only a small error need to be estimated, i.e. 5%.

The largest uncertainty will be found for the emissivity ε. Here we have two contributions

- measurement accuracy for the emissivity of the small sample at the laboratory in charge of the measurement (about 70%)
- error provision for the difference in emissivity between measured sample and real cryocover mirror (50%).

The straylight expected during ground test will have an uncertainty which is difficult to estimate due to

- the unknown uncertainty of the SPIRE filter scattering function (see chapter 4, this uncertainty is more important for the ground test than for the orbit case)
- the uncertain scattering function of the cryocover mirrors

We tentatively attribute uncertainties of 20% and 30% to these contributions (actually this value depends on the relation background/straylight). The sum for these roughly estimated individual errors is 195% (linear) and 96% (rss). So the numerical value of 25% for the accuracy is acceptable only as goal.

The present thermal design of the cryocover includes cooling devices providing a cool down to (nearly) LHe or LN temperatures depending on the cooling substance. Higher temperatures can be achieved easily, if the cooling flow is stopped; a slow warm up delivers a broad temperature range up to about 250 K. Should the warm-up speed be too quick for adequate testing, then the warm-up speed can be stopped/decreased by application of a low flux of the cooling flow. Thus a broad temperature range is available for the cryocover enabling an adjustment of the background to the needs. This also means that the optical power to be delivered can be adjusted over a broad range according to the request of the scientists during the test (guided by the internal calibration devices of the experiments themselves). So a relative accuracy of 25% is much more easily achievable than a corresponding absolute accuacy.

In addition to the emission from the telescope mirrors, there is the thermal emission of other objects in orbit (e.g. the hexapod, the cryostat elements etc.). Moreover, the recent emsisivity measurements on the telescope mirrors indicate very low emissivities, so the straylight correction may be quite important

either by selection of the planned emissivity for the cryocover mirrors
or by temperature increase during the ground test.

The planned sample program has been mentioned already

- special surface treatment of several mirror samples
- measurement of the emissivity in the far infrared at one of the laboratories cooperating with the project Herschel
- choice of the best surface treatment.

It is obvious that without such a program the achievement of the desired emissivity is pure speculation without any reasonable basis. This is the reason that only the design options with special surface treatment and sample program are acceptable.

4 Straylight from the Warm Objects during Ground Testing

4.1 Scatter Calculations

In general, the geometry is the same as for the orbit case (described in HP-2-ASED-TN-0023, issue 3), however, the cryocover is in its closed position.

The following objects

1) the ring of the CVV
2) the gap between this ring and the thermal shield 2 baffle (14.5 mm wide)
3) the short cone of the cryocover
4) the thermal shield 2 baffle
5) the gap above the instruments

have been set as emitting objects.

In addition to the list above, the contribution from the LOU via the gap 5) was calculated. The LOU radiation towards the gap 2) need not be calculated, since at that gap we already calculate with ambient temperature.

Geometry and calculational scheme from the LOU windows towards gap 5) are the same as described in HP-2-ASED-TN-0023, issue 3 (orbit case), with the following exception:

- The LOU emitting surfaces are located directly at the entrances of the 9 LOU baffle tubes.

The reason for that location is that the radiation from the CVV also comes through these holes around the LOU which (in this case) have the same temperature and effective emissivity.

The calculations for 1) through 5) involve two steps. First a purely specular calculation was done, i.e. no scattering function was assigned to any object. Since the cryocover mirrors were designed such that the experiments should see only themselves, no specular paths are expected. The corresponding calculation resulted in no significant specular paths for SPIRE and PACS.

For the second step several scattering functions were assigned to several objects. The corresponding functions for the surfaces on the cryocover and the thermal/instrument shields are plotted in the appendix in figures 5.1-1 to 5.1-3. The scattering functions for the experiments are the same as used for the calculations for the orbit case, see technical note HP-2-ASED-TN-0023 issue 3. They are plotted too in the appendix in figures 5.2-1 to 5.3-5. Compared to issue 1, new scattering functions for the SPIRE thermal filter 1 and the FP-unit have been received from SPIRE.

A review of the scattering functions revealed that the specific one for the cryocover mirrors (used in issue 1, also used up to the quarterly progress meeting July 2003) may have been too optimistic. Therefore the pessimistic one of the telescope mirrors is now applied instead. Consequently some small irradiance contributions now have increased, the small irradiances reported earlier for PACS have now surpassed the 1%-value. Also an increase of the gap width below the CVV and a temperature change of the thermal shield 2 baffle contribute to an increase in irradiance.

Some comments on the emissivities used for the calculations:

- the ring of the CVV has an emissivity of 0.05 (temperature 295 K)
- the gap between this ring and the thermal shield 2 baffle radiates quasi as black body (emissivity 0.9, temperature 291 K), since the MLI on the thermal shield 1 does not aquire the lower temperature of that shield and since the space between CVV and MLI is nearly closed
- the short cone of the cryocover shall be black in the thermal infrared; the anodizing process planned for that surface probably does not yield a black appearance for the scientific wavelengths, therefore an emissivity of 0.5 was selected (temperature 75 K)
- same comment for the emissivity of thermal shield 2 baffle as above (emissivity 0.5, temperature 50 K)
- the gap above the instruments and instrument shield is beneath a space nearly as closed as that mentioned above, so we set an emissivity of 0.9 (temperature 12 K).

The last gap does not play an important role. Nevertheless, the corresponding calculations are necessary for the calculation of the beam transport from the warm LOU windows.

The straylight calculations result in fluxes on the SPIRE and PACS detectors which are divided by the fluxes from both telescope mirrors. As usual, the contribution of the telescope mirrors has been set to 100 (telescope temperature 70 K, emissivity 0.015 for a single mirror). Corrections w.r.t. temperature and emissivity are applied, the results are shown in the next table. The values demonstrate that the straylight is substantially lower than the telescope contribution: This statement will also be true for a telescope with lower emissivity than used for comparison.

Table 4.1-1: Results of the straylight calculations for the ground tests, variant with concave reflecting cryocover mirrors, no misalignment.

Emitting object	**temperature/ emissivity**	**PACS detector**	**SPIRE detector**
CVV ring	295 K / 0.05	0.376	1.379
gap between CVV and thermal shield 2 baffle	291 K / 0.90	2.651	1.662
short outer cone of cryocover	75 K / 0.50	0.545	3.874
thermal shield 2 baffle	57 K / 0.50	1.140	1.552
gap between instrument shield and instruments	12 K / 0.90	0.035	0.192
LOU- and alignment-windows via gap between instrument shield and instruments	295 K / 0.90	0.389	0.098
sum		**5.14**	**8.76**

Data for PACS and SPIRE are in % with 100% = telescope irradiation (70 K, total ε=0.03)

Partly the difference between SPIRE and PACS is caused by the different position of the filter objects within the experiments. That of SPIRE is much more close to the experiment opening, thus it is irradiated to a higher degree than that of PACS. The irradiation of the SPIRE filter is also caused by the experiment walls of the so-called FP-UNIT which was assigned a reflectivity of 0.3.

Also the effect of misalignment was calculated. The cryocover mirrors were tilted by 40 arcmin around their nominal positions, the corresponding beam shifts on the experiment openings represent the effects of all angular and translational errors of the cryocover. This misalignment certainly is even stronger than the worse case to be expected from the budget listed in table 2.2-1 (chapter 2.2). A relative comparison

- calculations with misalignment of 40 arcmin
- calculations without misalignment

reveals that the resulting increase in straylight is moderate, the increase is roughly a third of the original straylight value. There is some scatter in the individual contributions, not all of them may be statistically significant. In summary, the moderate increase is tolerable.

A third step in the calculations involves the earlier variant of a black cryocover. The scattering function for the mirrors (figure 5.1-2) has to be replaced by a scattering function of a rough black surface. We use the same scattering function as used for the black shields, i.e. now figure 5.1-1 represents the black surfaces which are in the direct view of the experiments. Compared to issue 1 of this TN, further straylight paths have been calculated, especially the huge contribution from the thermal shield 2 baffle.

These calculations for this cryocover variant had been performed at an earlier time, the emissivity of the thermal shield 2 baffle was set to 0.8 instead of 0.5 used now. We did not repeat the calculations with the actual emissivity/reflectivity, since the evidence for the increase in straylight due to the increased scattering function of the black surface is convincing enough from the results shown in table 4.1-2 (compared to table 4.1-1). Clearly the version with black cryocover is not acceptable.

Table 4.1-2: Results of the straylight calculations during ground tests, variant with black cryocover

Emitting object	**temperature/ emissivity**	**PACS detector**	**SPIRE detector**
CVV	295 K / 0.05	8.63	2.43
gap betw. CVV and thermal shield 2 baffle	291 K / 0.90	76.25	20.09
short outer cone of cryocover	75 K / 0.50	8.35	6.06
thermal shield 2 baffle	57 K / 0.80	147.08	124.96
gap between instrument shield and instruments	12 K / 0.90	1.86	7.51
LOU- and alignment-windows via gap between instrument shield and instruments	295 K / 0.90	20.43	3.83
sum		**262.6**	**164.9**

Data for PACS and SPIRE are in % with 100% = telescope irradiation (70 K, total ε=0.03)

4.2 Diffraction Calculations

The diffraction calculations use the mecanical rims within the focal surface of the telescope as diffracting elements, in particular

- the rim of the SPIRE filter no. 1
- the rim of the PACS input aperture and the calibration rearview mirrors.

These rims are imaged onto the detector surfaces (just besides the detector rim, if no strong misalignment is present). This case is considered most important, because (due to the object-image relation between rim and detector) there may be a remarkable concentration of diffracted radiation on the detector. Thus there may be peaks in the local irradiance.

Diffraction from other rims (far away from the telscope focal surface) is spread across the detector surface, thus a peak in the local irradiance is unlikely. As will be shown later, only the possible peak in local irradiance requires most attention, the total flux averaged over the detector is negligible. This argument holds for most cases of the diffraction calculations (an exception is treated in the calculations for the orbit case, there diffraction at the rim of the secondary is of importance).

The calculations are done in four steps as explained in figures 4.2-1 through 4.2-3 for the case of SPIRE, the procedure for PACS is quite analogous. It is important to note that diffraction by several degrees cannot be calculated with ASAP in an automatic manner, since no ‘diffraction BSDF’ can be attributed to edges (as one could do for diffuse scattering by surfaces). ASAP’s coherent module (which yields diffracted radiation) does not work for diffraction by several degrees, also it requires that sufficient specific rays hit the surface where diffracted radiation is of interest. Therefore non-automatic calculational steps are necessary with appropriate simplifications to be made.

The first simplification allows for the fact that diffraction decreases strongly with diffraction angle (=angle between incident and diffracted ray). Consequently one concentrates on small diffraction angles as shown in figures 4.2-1 and 4.1-2. No diffraction was calculated for strongly inclined incident rays (i.e. zigzagging down to thermal filter 1), the corresponding diffraction angles would be much larger than those shown. Some rays zigzagging down to the PACS entrance are excluded now to a higher degree than done for the earlier calculations in June 2003.

Another simplification uses a set of 9 point sources on the emitting rings (CVV, CVV-gap etc.) instead of continuous emitting rings. Also the line source of step 3 is approximated by 9 point sources instead of a continuous line source; the corresponding graphs were smoothed along the line image.

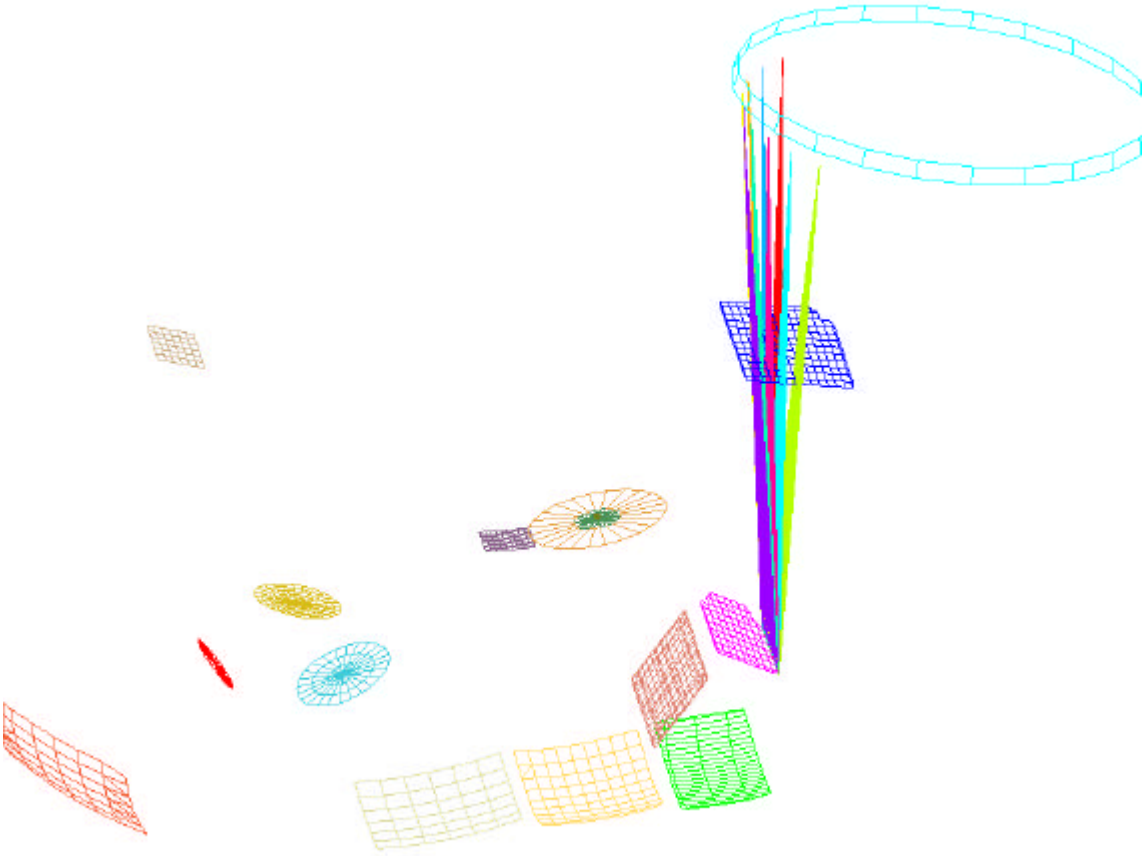

Figure 4.2-1: STEP 1 (of the diffraction calculations) consists of the calculation of the irradiance onto thermal filter 1 by the (partially warm) sources near the rim of the CVV. The trace is shown schematically with few rays, the calculations use much more rays. This figure only shows the optical elements of SPIRE for reasons of clarity; the case for PACS is analogous.

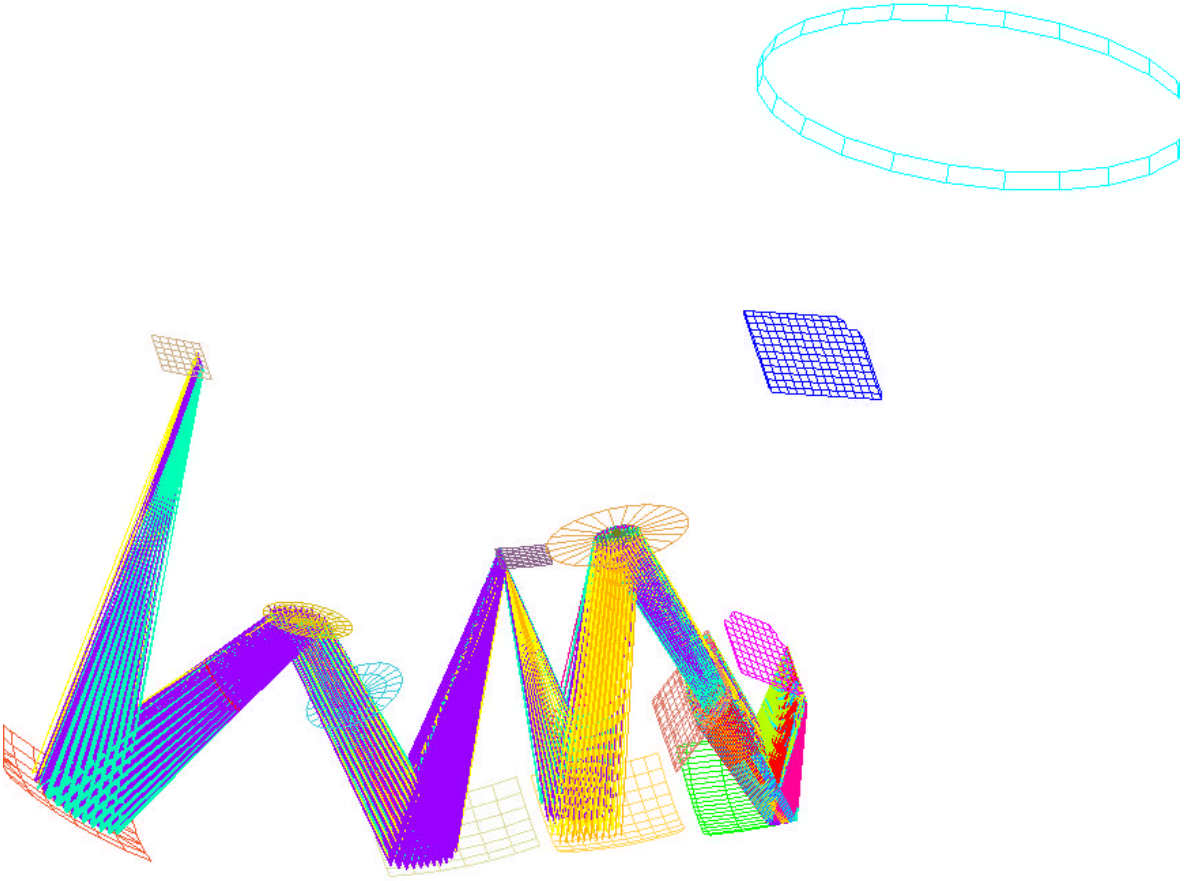

Figure 4.2-2: STEP 2 (of the diffraction calculations) consists of
- diffracted rays created at the rim of thermal filter 1
- ray directions and fluxes as from method of stationary phase
- flux of diffracted rays collected on detector.

Calculational problem:
rays converge outside rims of M6 and detector (by design), therefore M6 and the detector are enlarged; the collected flux, then, is an overestimation. Also the imager blur caused by beam limitation at the pupils is not obtained by the method of stationary phase dealing with diffraction at the rim of thermal filter 1. Both overestimations are corrected by steps 3 and 4.

Figure 4.2-2 only shows the optical elements of SPIRE for reasons of clarity; the case for PACS is analogous.

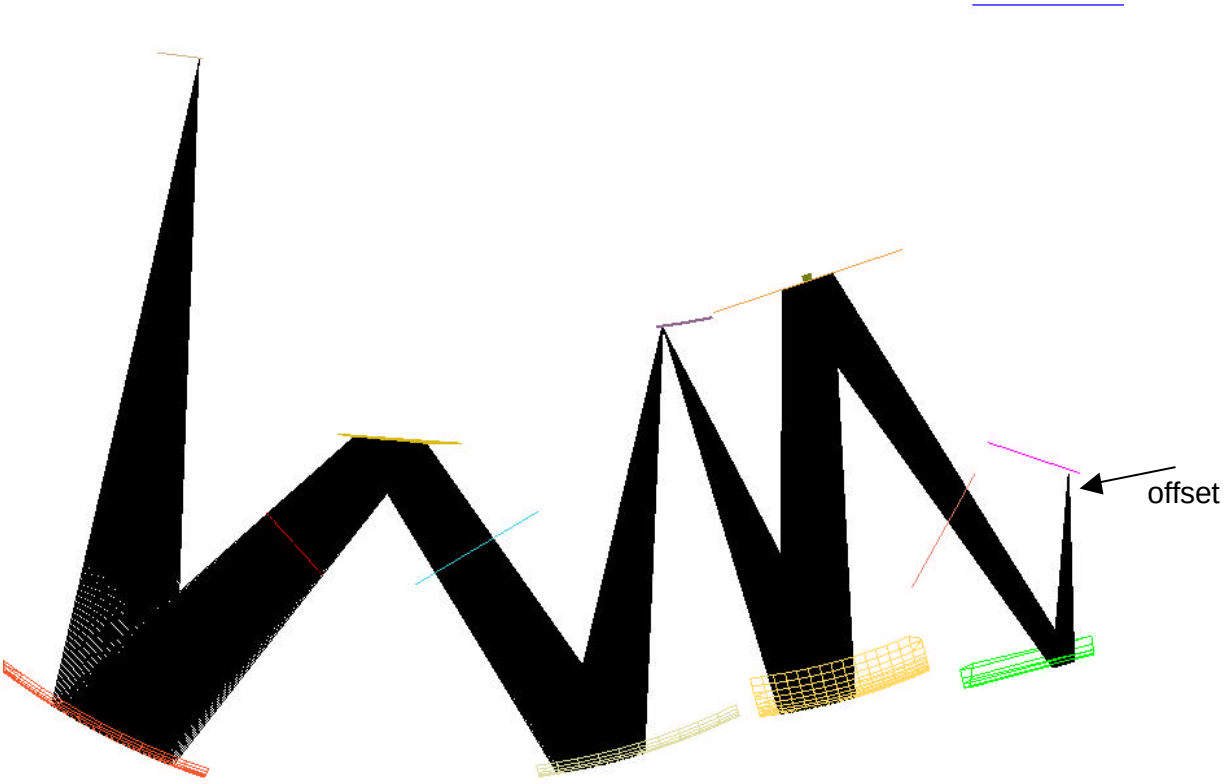

Figure 4.2-3: STEP 3 (of the diffraction calculations) consists of

- point sources (simulating a line source) are created within rim of thermal filter 1 with an offset value, this offset guarantees that beam limitation is done by the pupils
- therefore ASAP's coherent module can be used for finding the diffraction spread for the imaging from filter 1 to the detector (diffraction spread caused by beam limitation by the pupils)

The corresponding image on the detector still is an overestimation, since actually the peak of the image is outside the detector (by design). Therefore (in STEP 4) one shifts the rays on the detector by the scaled offset value mentioned above, so the peak now is outside the detector area as it is in reality. The resulting spreaded image now is a steep ramp.

Figure 4.2-3 only shows the optical elements of SPIRE for reasons of clarity; the case for PACS is analogous.

Figures 4.2-4 through 4.2-7 show the resulting irradiance distributions on the detectors of SPIRE and PACS. They represent the diffraction at the rim on the +Z-side of the corresponding opening in the experiment (w.r.t. the center of that opening). This is a single specific case, not an average of several cases. The choice for the +Z-side was done because

- the margins along Z are smaller than those along Y
- the relevant irradiance was estimated to be strong.

The irradiances presented in the figures are not normalized (mainly due to calculational reasons, the final normalization was done outside the calculational sequence within ASAP). So the reader is asked to view these irradiance distributions only as a relative information. However, the following table presents normalized irradiances, so the desired comparison with the reference irradiance of the telescope mirrors indeed is possible with the aid of these tables.

The scale in mm on the graphs depends on the detector size chosen for the specific (simplified) ASAP model. For better evaluation, the scale factors are given here:

- the SPIRE detector in ASAP has the scale 1 mm ⇔ 12.76 arcsec on sky
- the PACS detector in ASAP has the scale 1 mm ⇔ 5.98 arcsec on sky.

Some comments on the emitting elements and the emissivities/temperatures selected for the calculations

- the ring of the CVV has an emissivity of 0.05 (temperature 295 K)
- the gap between this ring and the thermal shield 2 baffle radiates quasi as black body (emissivity 0.9, temperature 291 K), since the MLI on the thermal shield 1 does not aquire the lower temperature of that shield and since the space between CVV and MLI is nearly closed
- the short cone of the cryocover shall be black in the thermal infrared; the anodizing process planned for that surface probably does not yield a black appearance for the scientific wavelengths, therefore an emissivity of 0.5 was selected (temperature 75 K)
- same comment for the emissivity of thermal shield 2 baffle as above (emissivity 0.5, temperature 50 K)
- the gap above the instruments does not play an important role.

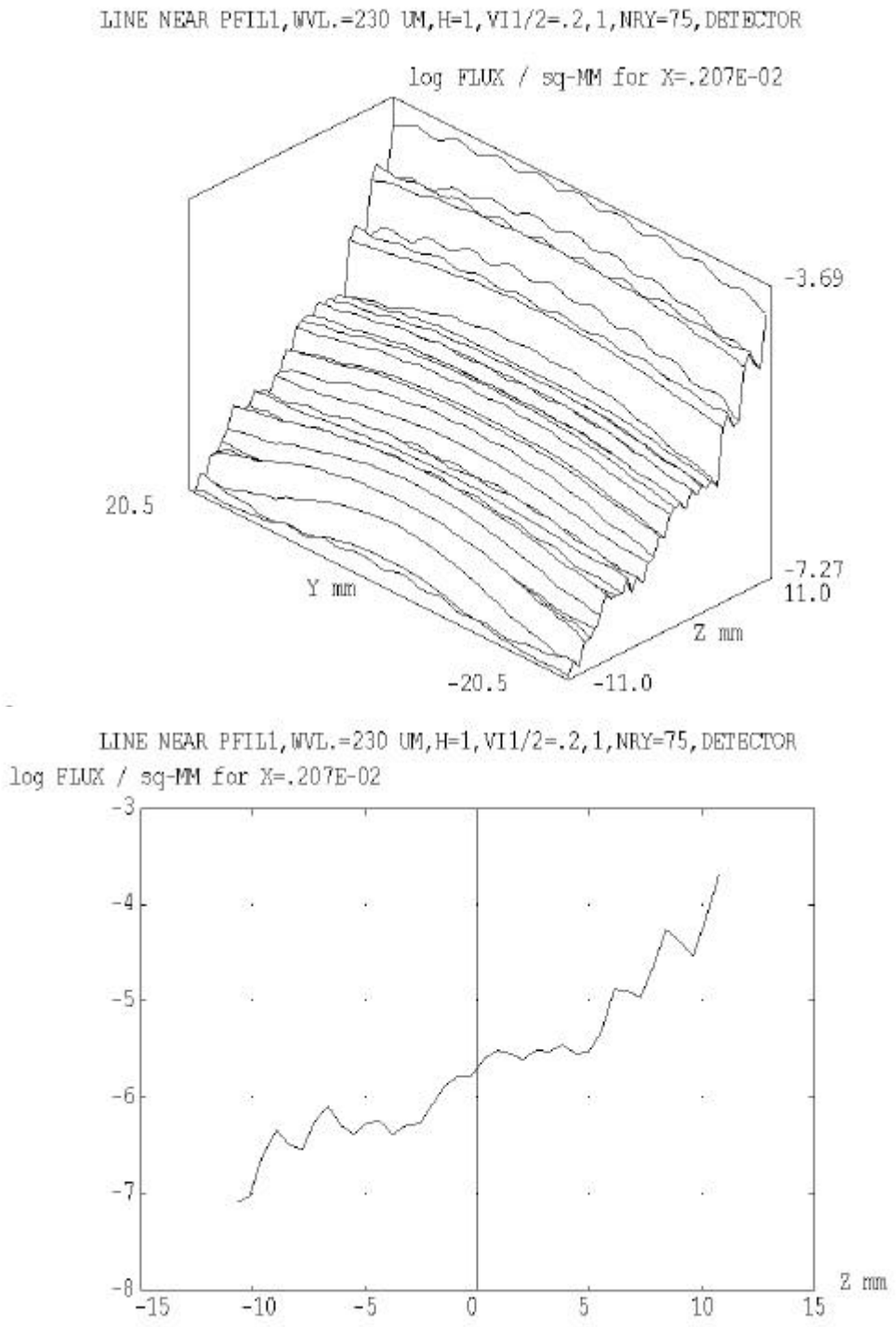

Figure 4.2-4: Irradiance distributions across the SPIRE detector (logarithmic ordinate) for case of

- irradiance by the (partially warm) sources near the CVV rim
- diffraction at the rim of the +Z-side of the SPIRE filter no. 1 (w.r.t. the center of that filter)
- wavelength 230 micrometer.

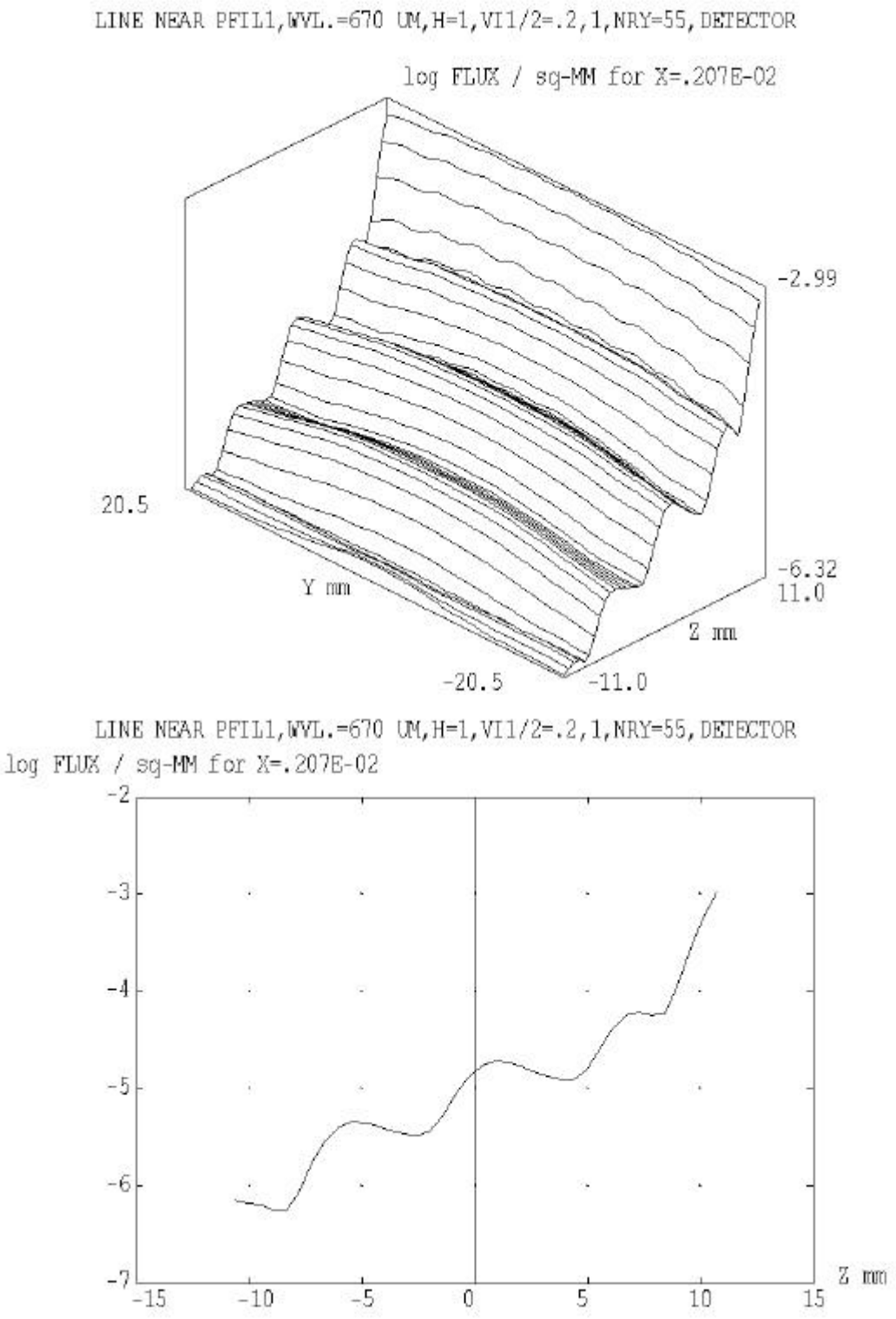

Figure 4.2-5: Irradiance distributions across the SPIRE detector (logarithmic ordinate) for case of

- irradiance by the (partially warm) sources near the CVV rim
- diffraction at the rim of the +Z-side of the SPIRE filter no. 1 (w.r.t. the center of that filter)
- wavelength 670 micrometer.

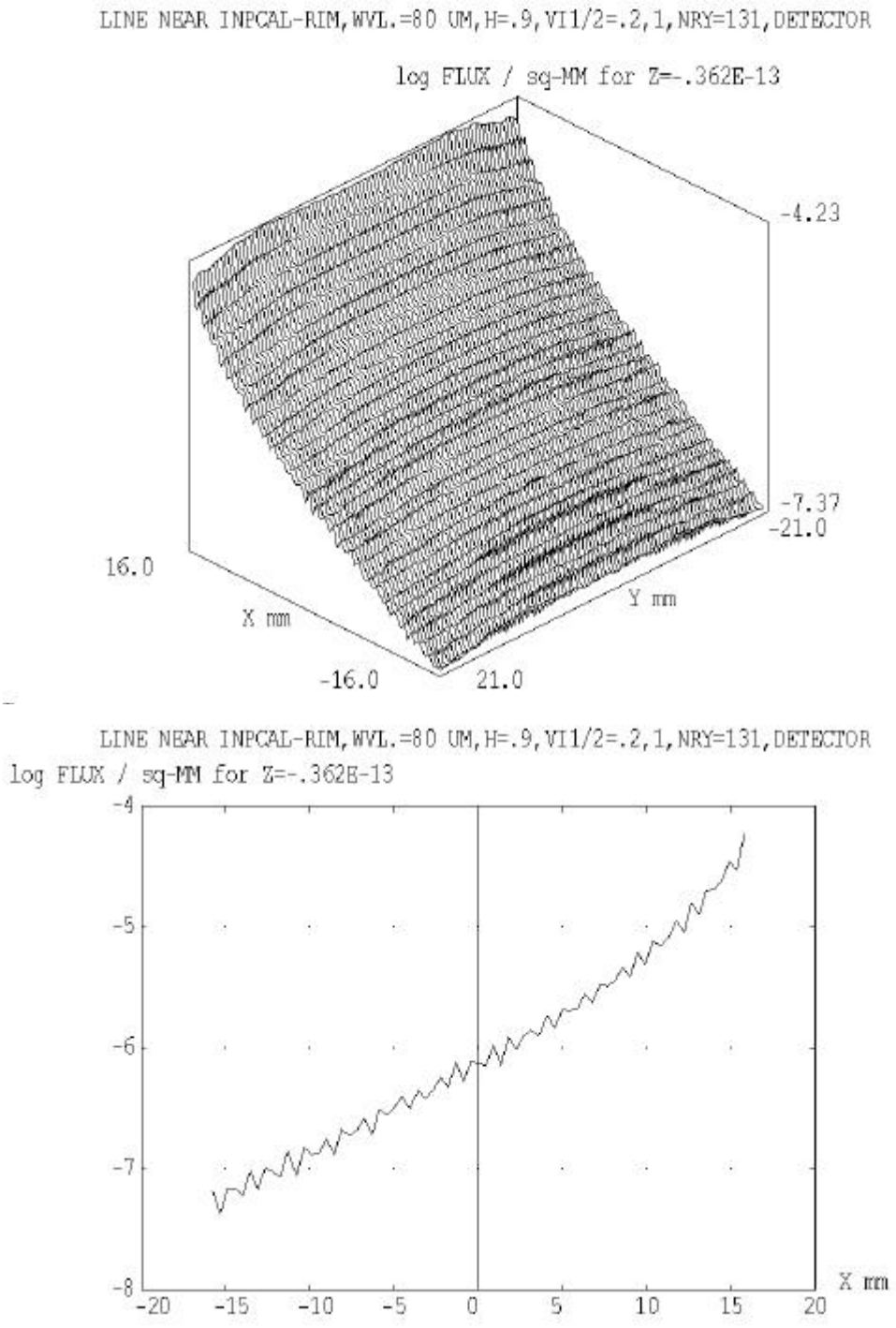

Figure 4.2-6: Irradiance distributions across the PACS detector (logarithmic ordinate) for case of

- irradiance by the (partially warm) sources near the CVV rim
- diffraction at the rim of the +Z-side of the PACS opening (w.r.t. the center of that opening)
- wavelength 80 micrometer.

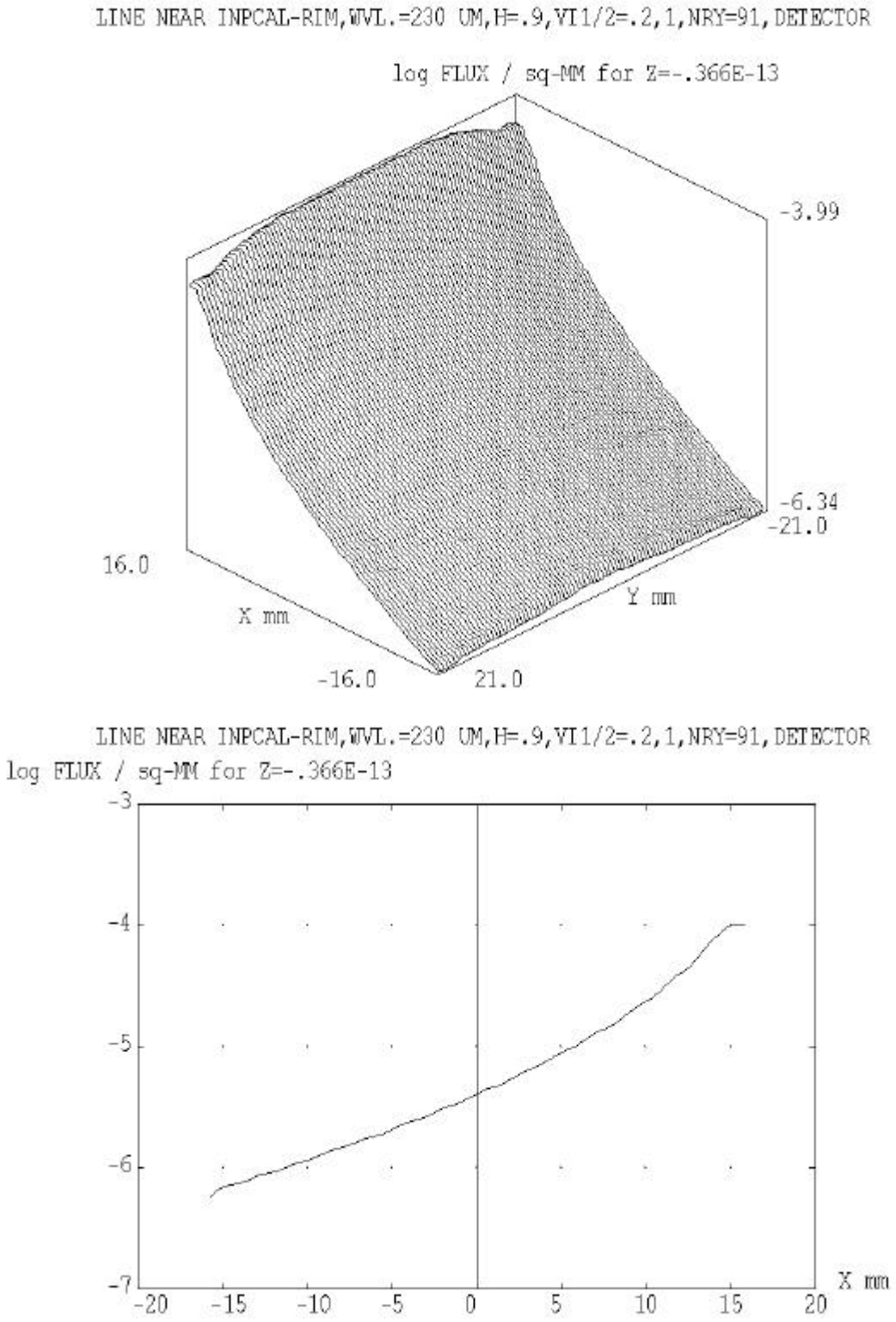

Figure 4.2-7: Irradiance distributions across the PACS detector (logarithmic ordinate) for case of
- irradiance by the (partially warm) sources near the CVV rim
- diffraction at the rim of the +Z-side of the PACS opening (w.r.t. the center of that opening)
- wavelength 230 micrometer.

Table 4.2-1 shows the normalized irradiances on the detector (aiding the interpretation of the preceeding graphs).

emitting object	CVV rim (295 K, ε=0.05)		gap below CVV (291 K, ε=0.9)		black cone on cryocover (75 K, ε=0.5)		baffle of thermal shield 2 (57 K, ε=0.5)		sum of all objects	
diffraction at a single rim (at +Z-side) of thermal filter 1 of SPIRE										
irradiance onto detector	230µm	670µm	230µm	670µm	230µm	670µm	230µm	670µm	230µm	670µm
maximum	0.0544	0.6246	0.0445	0.5109	0.1094	1.5698	0.0410	0.6582	0.2493	3.3635
average	0.0029	0.0344	0.0024	0.0281	0.0058	0.0863	0.0022	0.0362	0.0132	0.1850
minimum	0.0000	0.0003	0.0000	0.0002	0.0000	0.0007	0.0000	0.0003	0.0001	0.0016
diffraction at a single rim (at +Z-side) of PACS input (plane of rearview mirrors)										
irradiance onto detector	80 µm	230µm	80 µm	230µm	80 µm	230µm	80 µm	230µm	80 µm	230µm
maximum	0.0015	0.0031	0.0198	0.0418	0.0013	0.0061	0.0024	0.0159	0.0250	0.0668
average	0.0001	0.0004	0.0015	0.0056	0.0001	0.0008	0.0002	0.0021	0.0018	0.0089
minimum	0.0000	0.0000	0.0000	0.0002	0.0000	0.0000	0.0000	0.0001	0.0000	0.0003

Table 4.2-1: Results for diffraction at a rim within an image plane during ground testing
Case with line images outside the detector area (no appreciable misalignment).
Data for PACS and SPIRE are in % with 100% = telescope irradiation (70 K, total ε=0.03)

The irradiances listed in the preceeding table actually occur at 4 sides of the detector (not only the one shown in the graph). The corresponding average values still are negligibly small.
This is also true, if another diffracting edge is taken into account (e.g. the input edge of SPIRE, the input edge of PACS). Although irradiation and diffraction effect varies from edge to edge, there is enough margin for that statement. Not all edges contribute appreciably to diffraction, since not all are irradiated by strong sources.

So, in general, the diffraction at edges close to the experiment openings are considered to have no appreciable effect. Exception: For SPIRE the increase of irradiance towards the detector rim is not negligible at the longest wavelengths, there an apparent irradiated rim of 4…10% has to be expected.

All statements above rely on the condition that the detectors do not have a view onto those edges which are irradiated appreciably (near experiment openings). Misalignments (also within experiments) must not destroy this avoidance. The case of misalignments is treated in the next chapter.

4.3 Diffraction Calculations in Connection with Misalignment / Chopping

This chapter reports on cases where the ideal alignment status within the experiment is not present. For SPIRE, a misalignment mainly will shift the bright line image closer to the detector rim, hopefully not across that rim. However, in order to display the full diffraction ramp, the figures presented here (in chapter 4.3 only) assume such a large misalignment that the maximum is clearly visible on the detector. The reader, then, is able to assess all intermediate states between perfect and bad alignment status. In fact, the graphs displayed here are the result of all calculational steps of figures 4.2-1 through 4.2-3, but without step 4.

The resulting diffraction images for SPIRE are shown in figures 4.3-1 and 4.3-2. As mentioned for chapter 4.2, the irradiances presented here are not normalized too (mainly due to calculational reasons, the final normalization was done outside the calculational sequence within ASAP). So again the reader is asked to view these irradiance distributions only as a relative information. However, the following table presents normalized irradiances, so the desired comparison with the reference irradiance of the telescope mirrors indeed is possible with the aid of these tables.

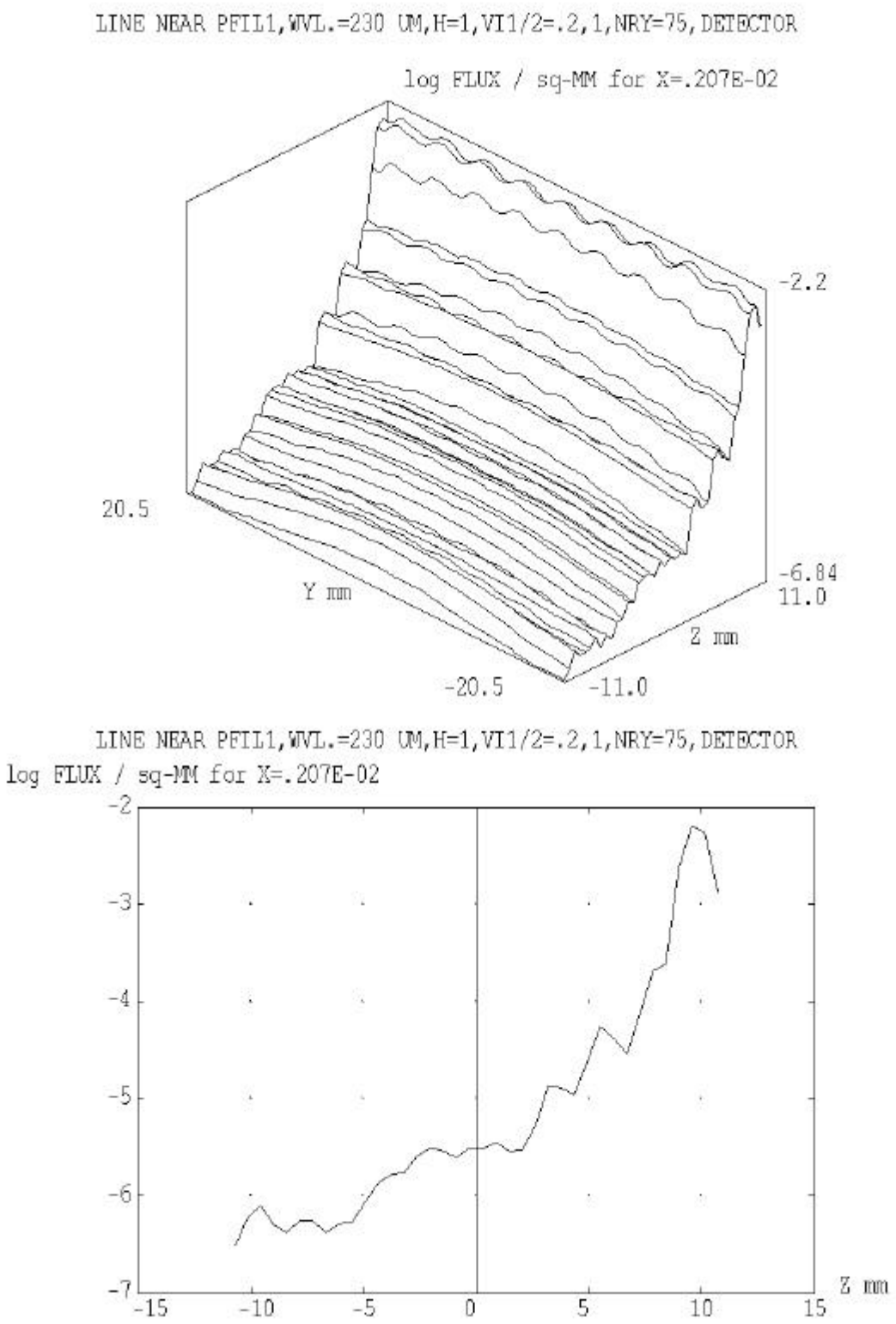

Figure 4.3-1: Irradiance distributions across the SPIRE detector (logarithmic ordinate) for case of

- irradiance by the (partially warm) sources near the CVV rim
- diffraction at the rim of the +Z-side of the SPIRE opening (w.r.t. the center of that opening)
- wavelength 230 micrometer
- line image on detector area (e.g. by misalignment).

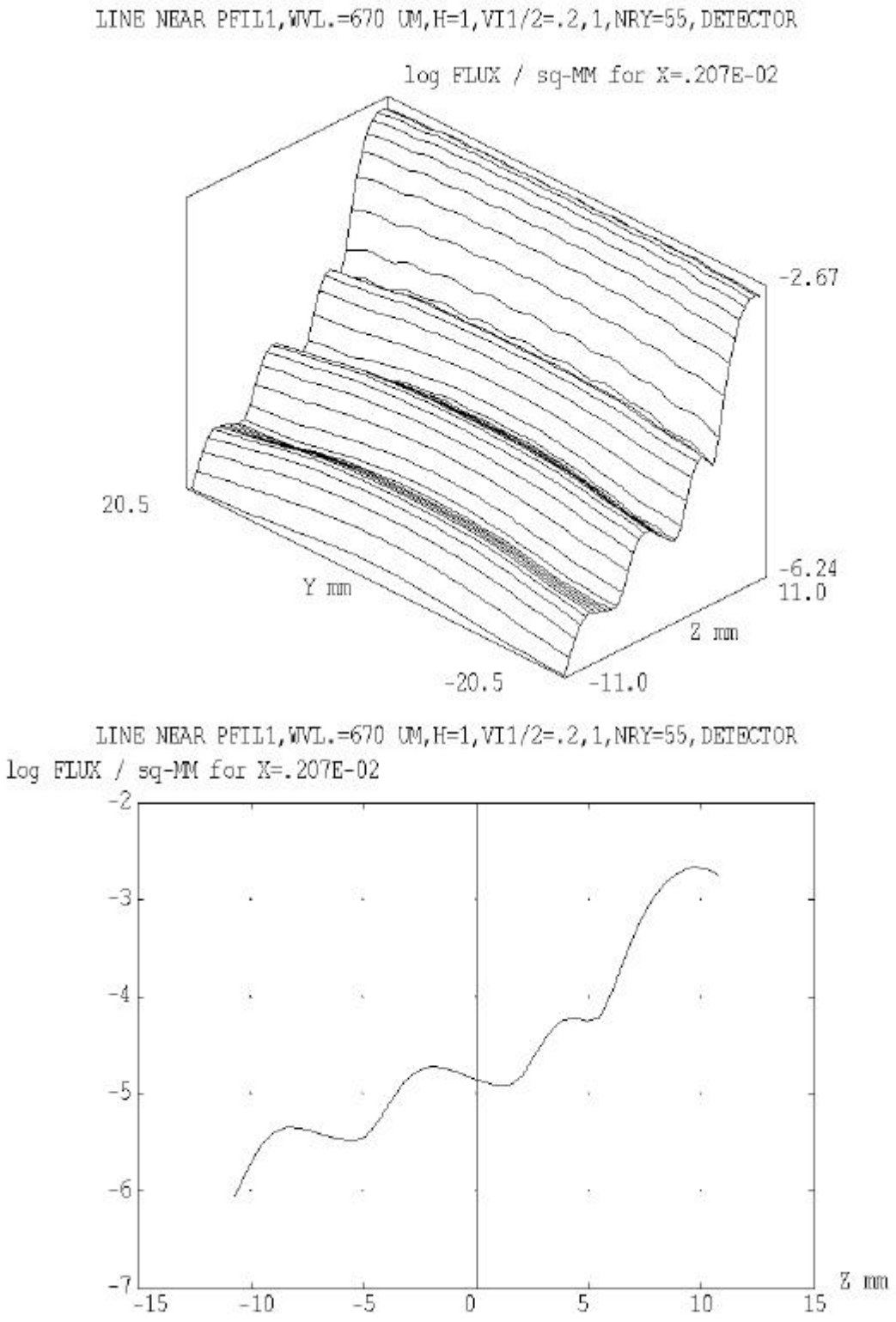

Figure 4.3-2: Irradiance distributions across the SPIRE detector (logarithmic ordinate) for case of

- irradiance by the (partially warm) sources near the CVV rim
- diffraction at the rim of the +Z-side of the SPIRE opening (w.r.t. the center of that opening)
- wavelength 670 micrometer
- line image on detector area (e.g. by misalignment).

For PACS the situation is somewhat different. The misalignments may also shift the bright line image closer to the detector rim. In addition there is a chopper action sweeping the beam along Y-direction towards the rearview mirrors of the calibration paths. When sweeping from orbit field to calibration field, the rim of the rearview mirror is crossed, i.e. the line image crosses the whole field of the detector. Therefore the graphs for PACS display the bright line image in the center, i.e. consistent with an action of the chopper for reaching the calibration beams. An inconsistency exists with the calculated geometry

- the calculations use a diffracting rim at +Z-side w.r.t the center of the PACS opening
- the rearview mirrors provide diffracting rims at +-Y-side w.r.t the center of the PACS opening.

The calculations had been programmed for the +Z-case, since there smaller margins exist (especially for SPIRE). When ‘applying’ the graphs (gained for the +Z-case) to the case of chopping along +-Y in PACS, one clearly applies a rough approximation (figures 4.3-4 and 4.3-5), but the order of magnitude should be correct.

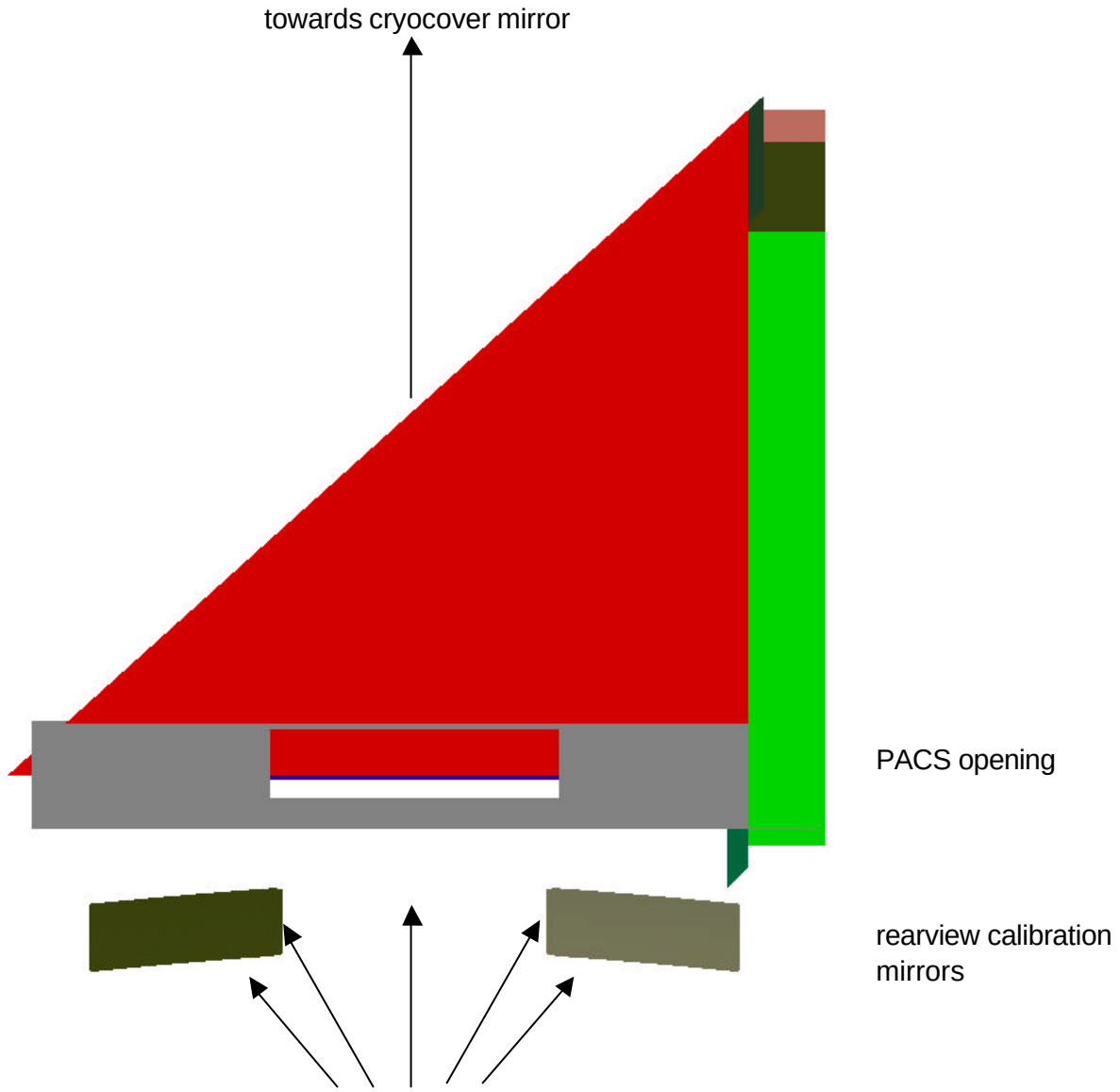

Figure 4.3-3: The rims of the PACS calibration rearview mirrors are crossed by the beam during chopping towards calibration paths

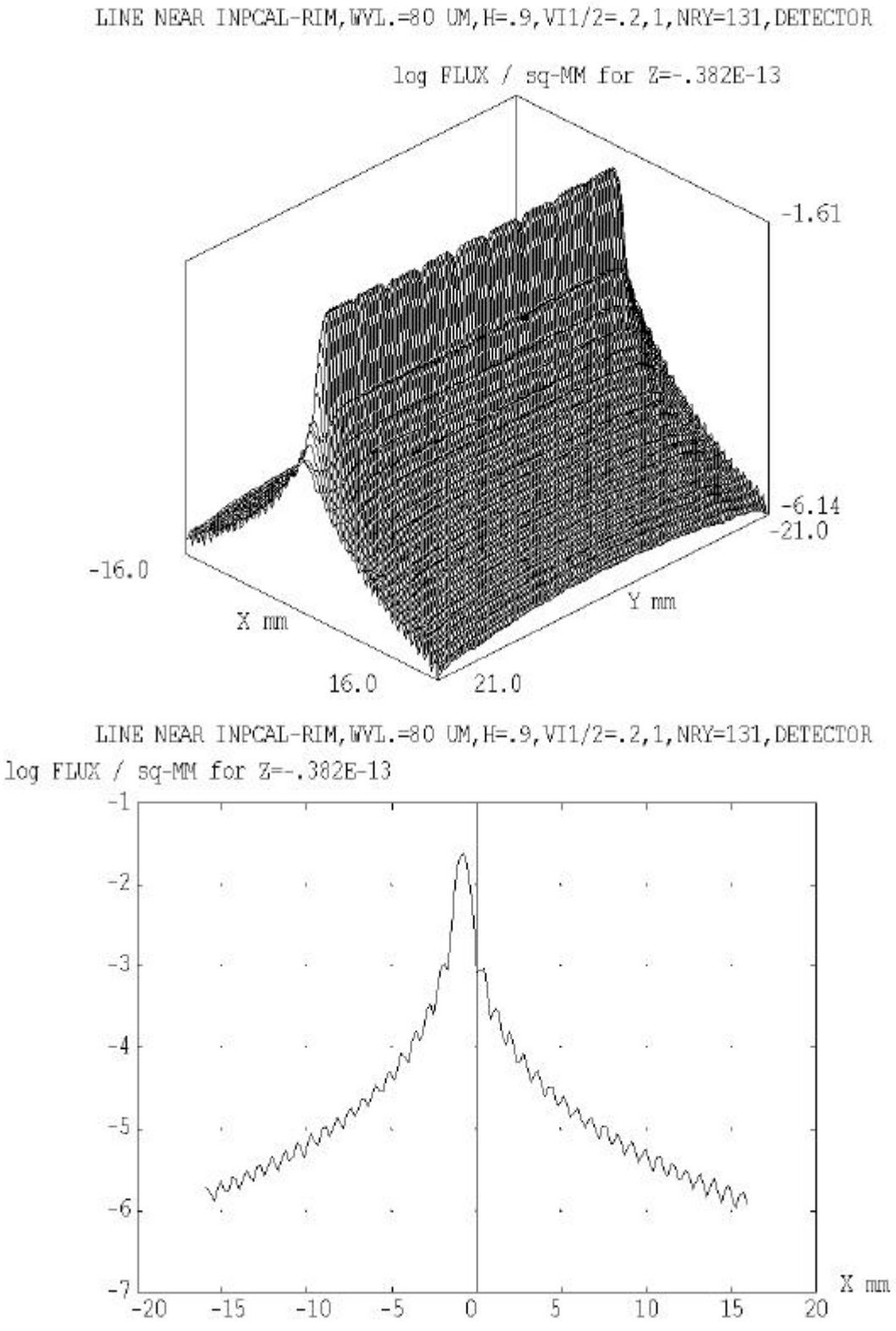

Figure 4.3-4: Irradiance distributions across the PACS detector (logarithmic ordinate) for case of

- irradiance by the (partially warm) sources near the CVV rim
- diffraction at the rim of the +Z-side of the PACS opening (w.r.t. the center of that opening)
- wavelength 80 micrometer
- line image at center (e.g. by chopping action).

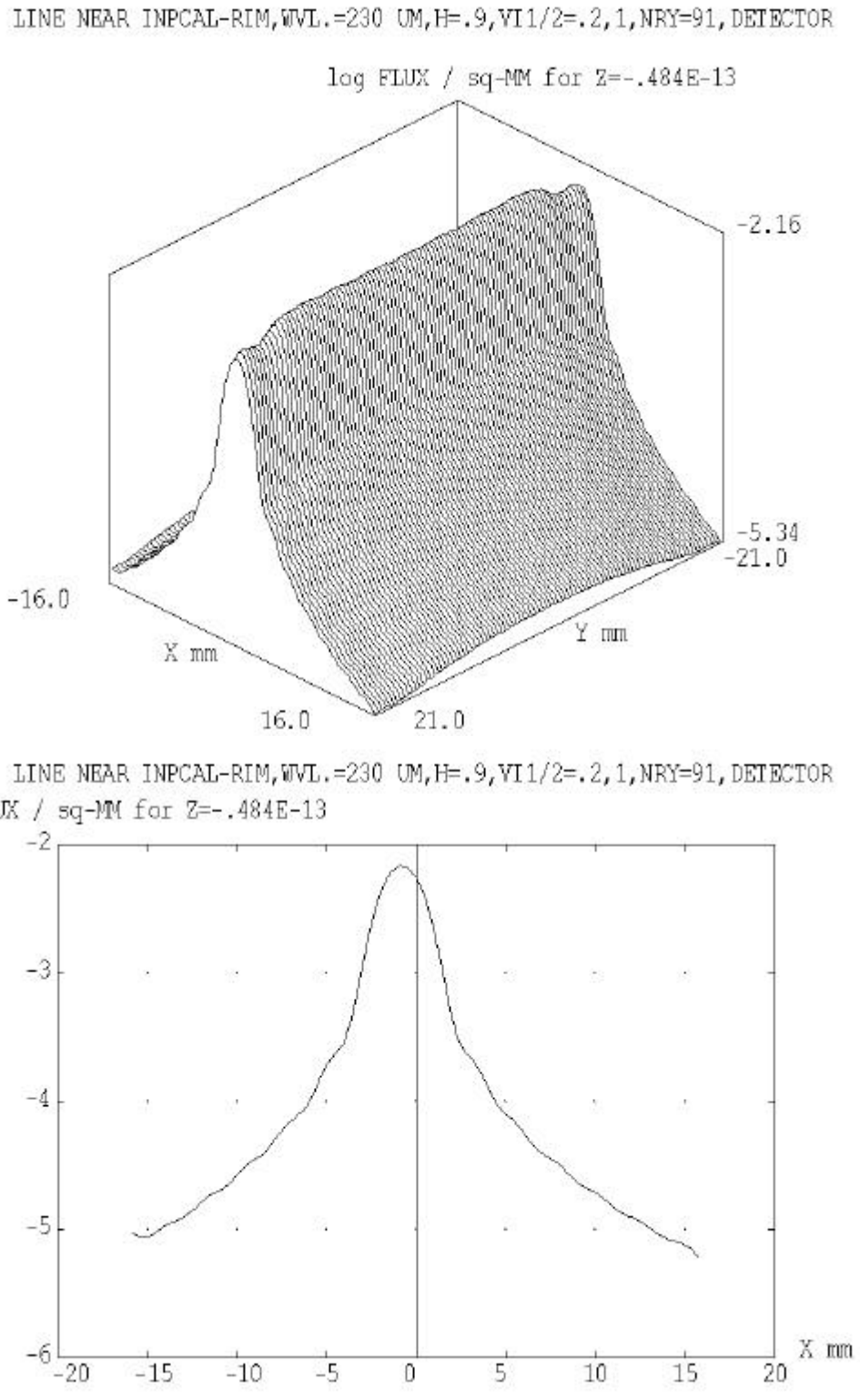

Figure 4.3-5: Irradiance distributions across the PACS detector (logarithmic ordinate) for case of

- irradiance by the (partially warm) sources near the CVV rim
- diffraction at the rim of the +Z-side of the PACS opening (w.r.t. the center of that opening)
- wavelength 230 micrometer
- line image at center (e.g. by chopping action).

Table 4.3-1 shows the normalized irradiances on the detector (aiding the interpretation of the preceeding graphs).

emitting object	CVV rim (295 K, ε=0.05)		gap below CVV (291 K, ε=0.9)		black cone on cryocover (75 K, ε=0.5)		baffle of thermal shield 2 (57 K, ε=0.5)		sum of all objects	
diffraction at a single rim (at +Z-side) of thermal filter 1 of SPIRE										
irradiance onto detector	230µm	670µm	230µm	670µm	230µm	670µm	230µm	670µm	230µm	670µm
maximum	1.7009	1.3152	1.3931	1.0760	3.4214	3.3058	1.2838	1.3861	7.7991	7.0831
average	0.0928	0.1779	0.0760	0.1455	0.1868	0.4471	0.0701	0.1874	0.4257	0.9579
minimum	0.0000	0.0003	0.0000	0.0003	0.0001	0.0009	0.0000	0.0004	0.0002	0.0019
diffraction at a single rim (at +Z-side) of PACS input (plane of rearview mirrors)										
irradiance onto detector	80 µm	230µm	80 µm	230µm	80 µm	230µm	80 µm	230µm	80 µm	230µm
maximum	0.6109	0.2553	8.2561	3.4639	0.5552	0.5018	0.9962	1.3196	10.418	5.5406
average	0.0150	0.0184	0.2024	0.2493	0.0136	0.0361	0.0244	0.0950	0.2554	0.3987
minimum	0.0000	0.0001	0.0002	0.0016	0.0000	0.0002	0.0000	0.0006	0.0003	0.0025

Table 4.3-1: Results for diffraction at a rim within an image plane during ground testing
Case with line images shifted into the detector area (misalignment or chopping).
Data for PACS and SPIRE are in % with 100% = telescope irradiation (70 K, total ε=0.03)

No judgement of these results is given here, since

- the probability of appreciable experiment internal misalignment cannot be given by industry
- the presence of the bright line image during chopping towards the calibration mirrors has to be judged by PACS.

No diffuse scattering from the rims (dealt with both in chapters 4.2 and 4.3) has been calculated. The scattering behaviour certainly depends much on the shape and size of the rims (sharp, round?). Nevertheless, in the far infrared the relation between rim size and wavelength is favourable.

5 Appendix: Scattering Models used for the Calculations

The following pictures show the scattering models used for the calculations.

Models for Cyostat parts (Figures 5.1-1 through 5.1-3)
PACS scatter model (Figure 5.2-1)
SPIRE scatter models (Figures 5.3-1 through 5.1-5)

In addition, a Lambertian model (BSDF=0.1/π per sr) was used for

- the filter in the PACS pupil (in transmission)
- PACS mechanics around the PACS opening.

(model not shown as picture).

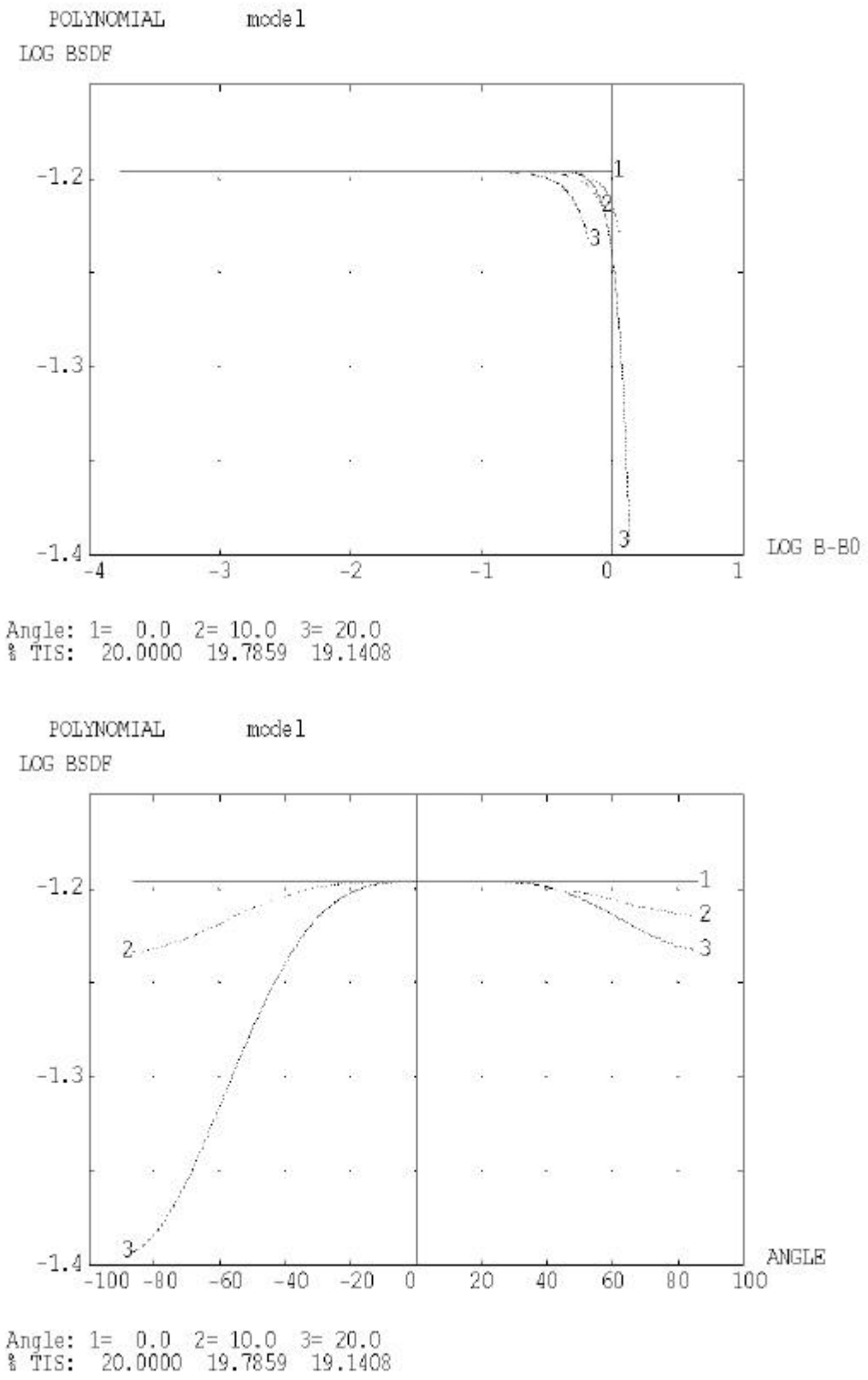

Fig. 5.1-1: Model for thermal shield 2 baffle and instrument shield baffle tube
(also for deleted black flat cryocover variant)
(POLYNOMIAL 2 2 LOG[.2/3.1416] 5@0, 0 0 1.8 0 0 1.8, 0 -1.8)
The upper plot mainly shows the values for small scattering angles
The lower plot mainly shows the values for large scattering angles

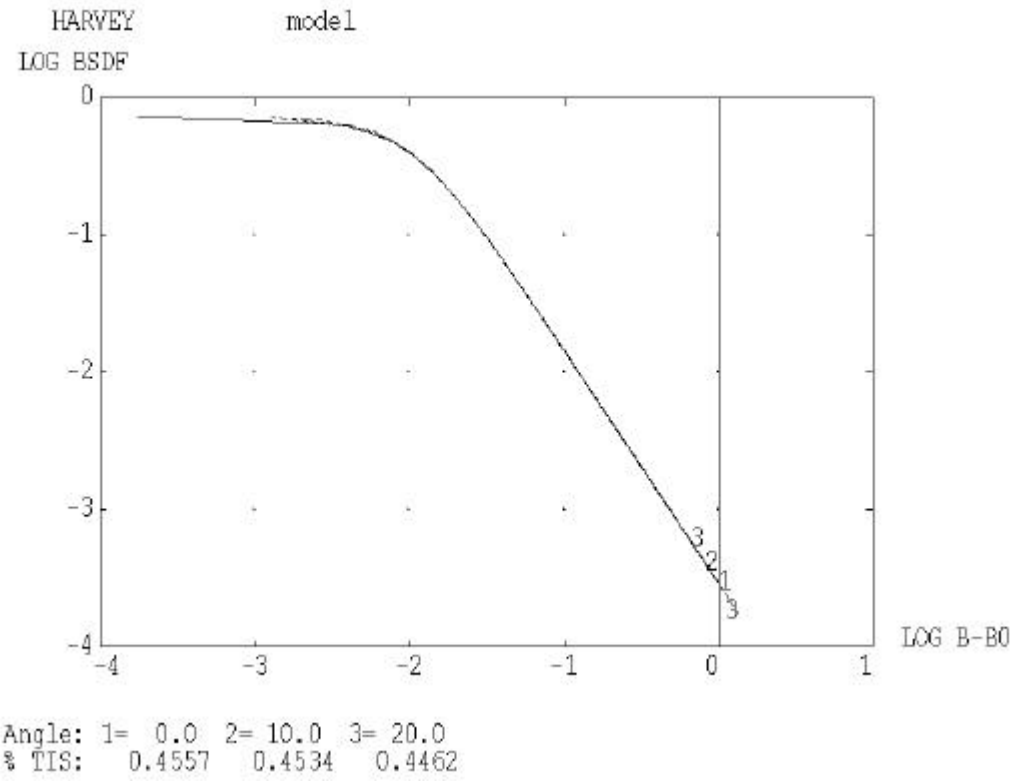

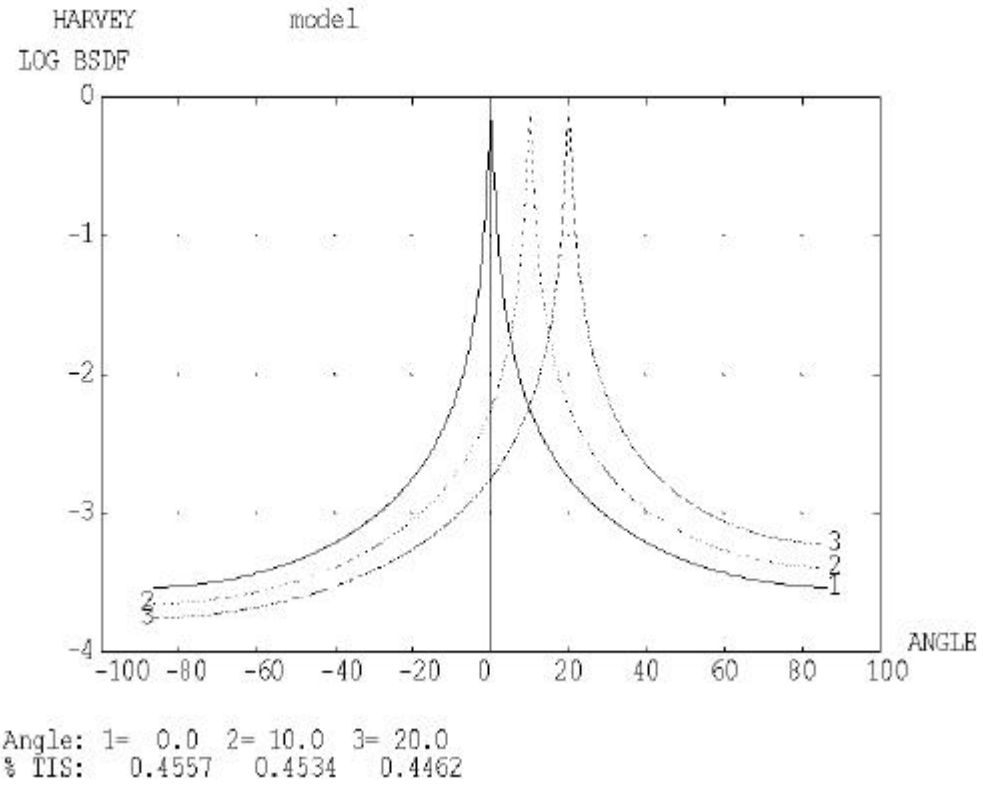

Fig. 5.1-2: Model for cryocover mirrors, Harvey 0.73 -1.7 0.01
The upper plot mainly shows the values for small scattering angles
The lower plot mainly shows the values for large scattering angles

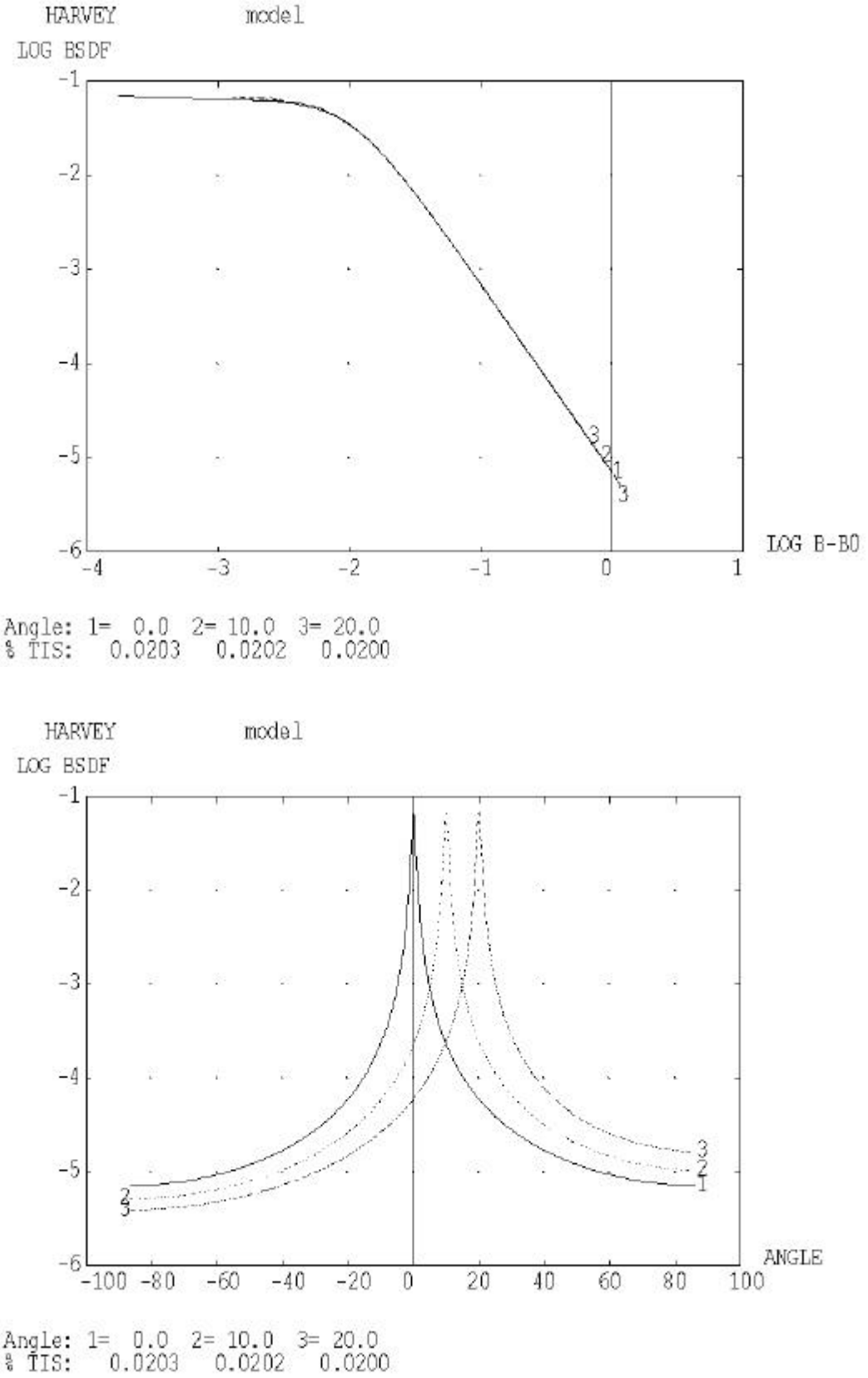

Fig. 5.1-3: Model for instrument shield flat and flat cryocover parts, Harvey 0.07 -2 0.01
The upper plot mainly shows the values for small scattering angles
The lower plot mainly shows the values for large scattering angles

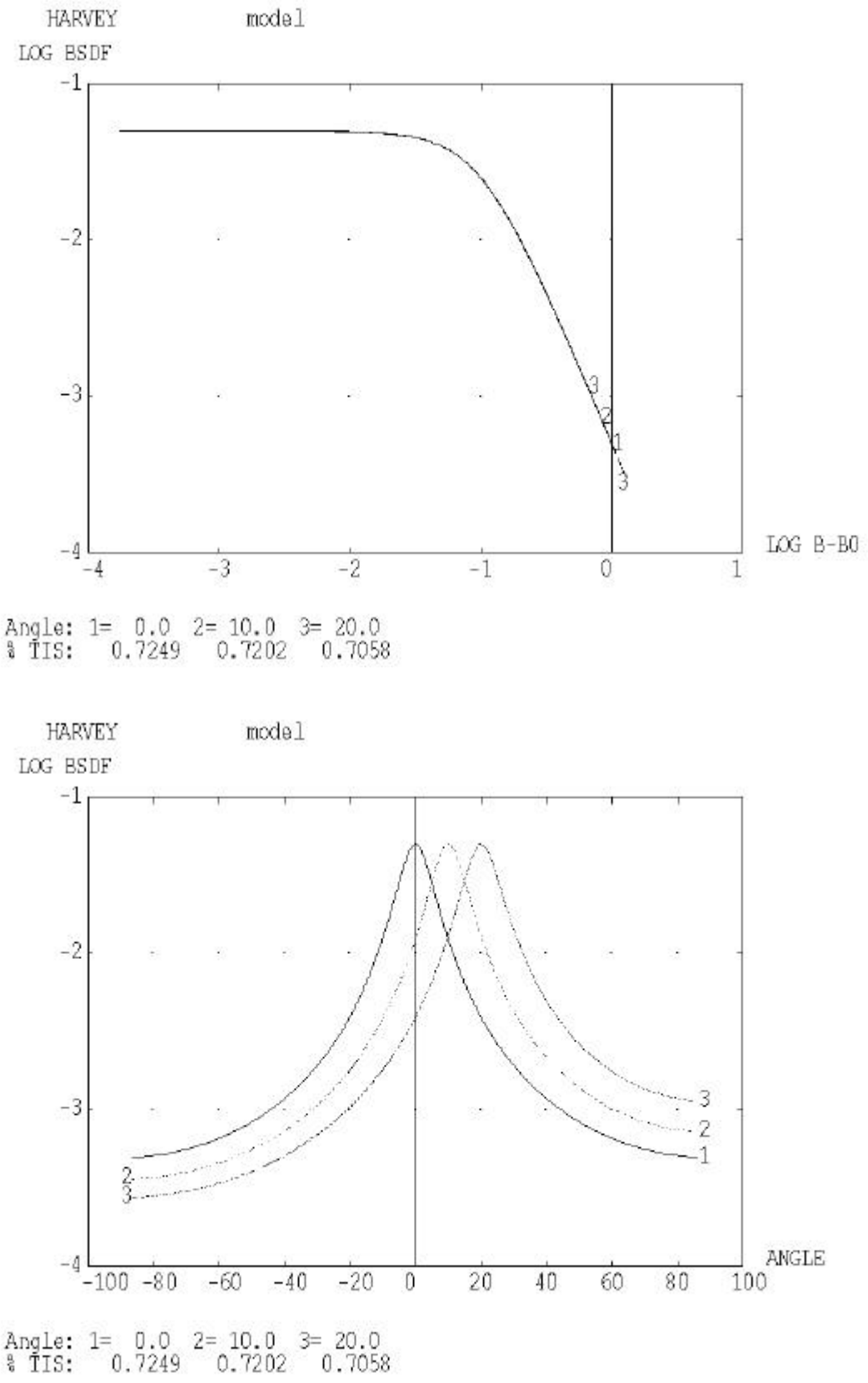

Fig. 5.2-1: Model for PACS Trog1, Trog2, Trog3, Fold1, Harvey 0.05 -2 0.1
The upper plot mainly shows the values for small scattering angles
The lower plot mainly shows the values for large scattering angles

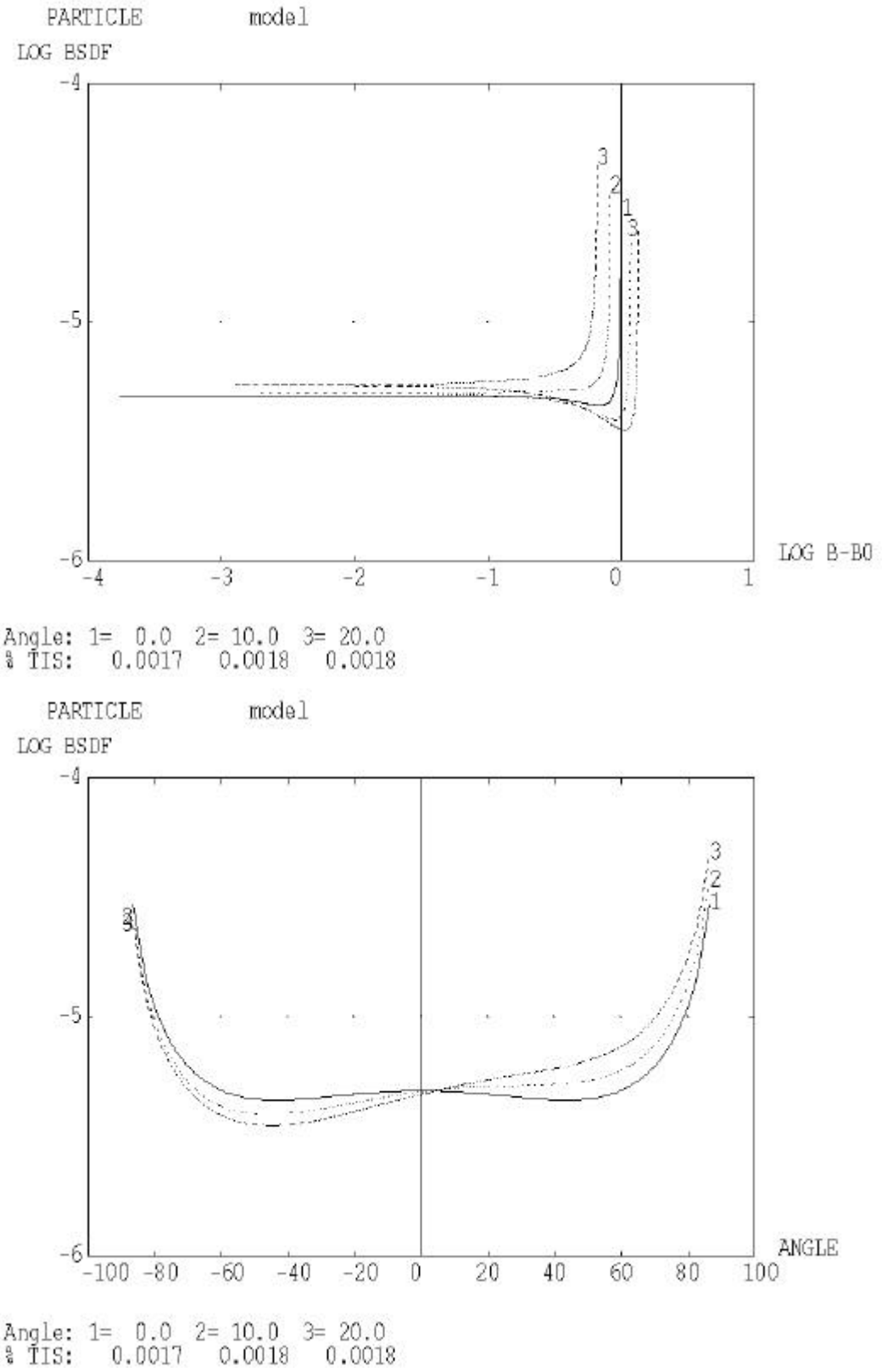

Fig. 5.3-1: Model for SPIRE M3 (particle model),
The upper plot mainly shows the values for small scattering angles
The lower plot mainly shows the values for large scattering angles

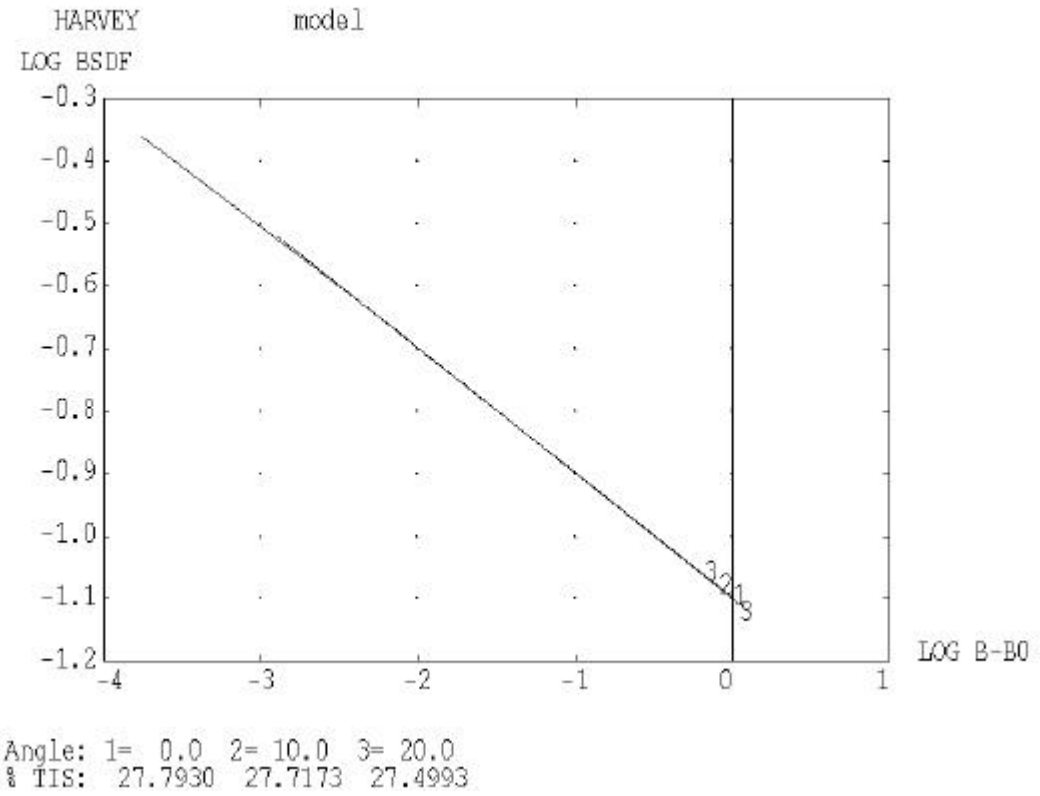

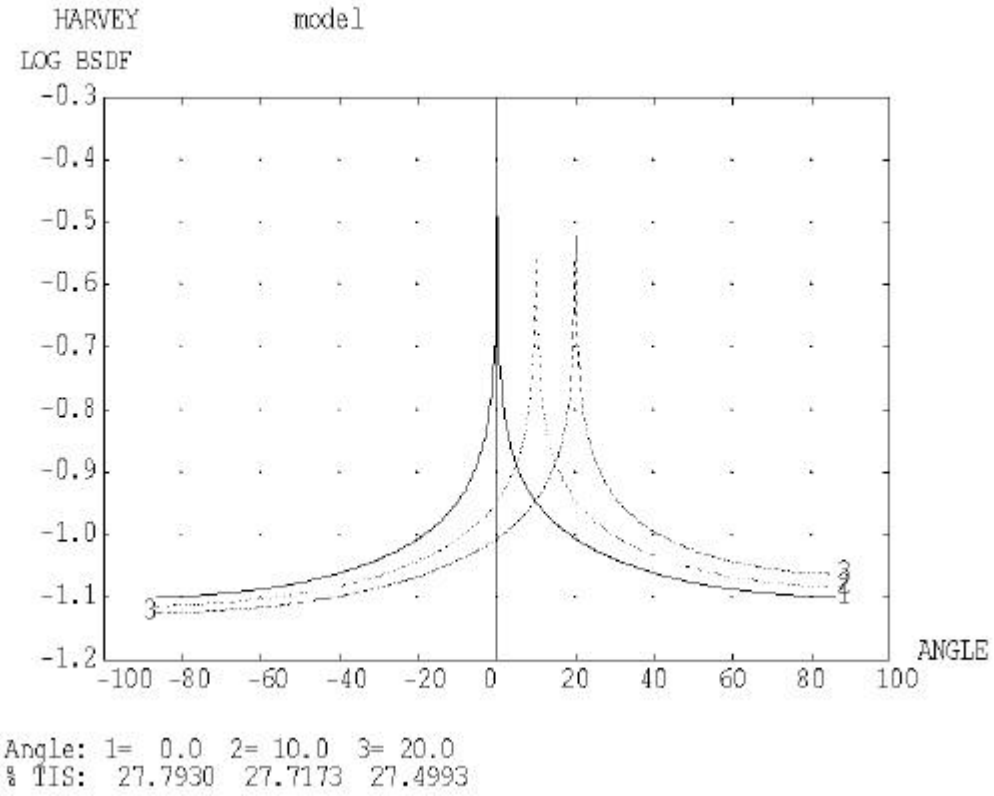

Fig. 5.3-2: Model for SPIRE M4 aperture (i.e. mechanics around M4), Harvey 0.2 -0.2
The upper plot mainly shows the values for small scattering angles
The lower plot mainly shows the values for large scattering angles

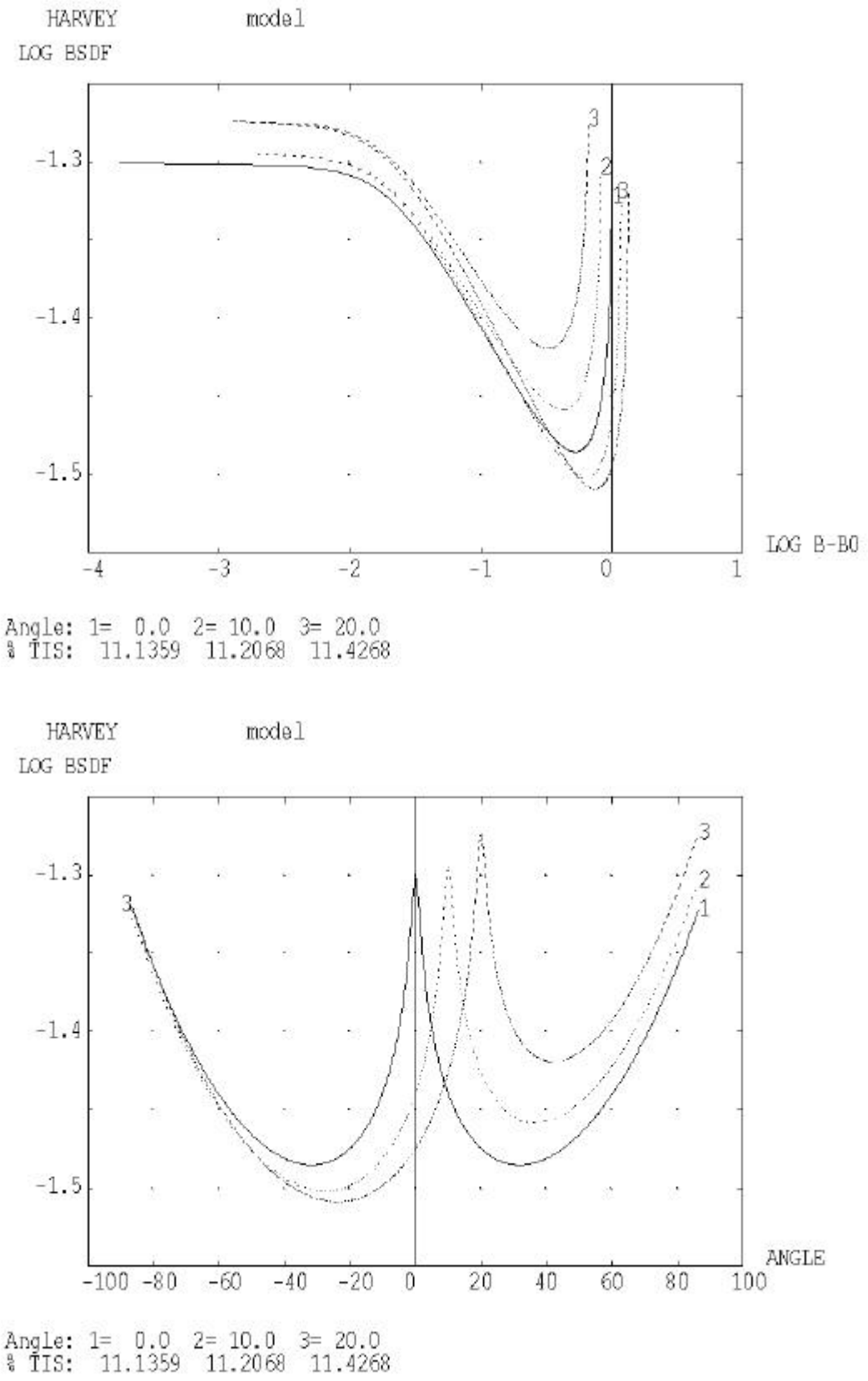

Fig. 5.3-3: Model for SPIRE FP_UNIT, upper part, HARVEY 0.05 -0.15 0.02 1 1
The upper plot mainly shows the values for small scattering angles
The lower plot mainly shows the values for large scattering angles

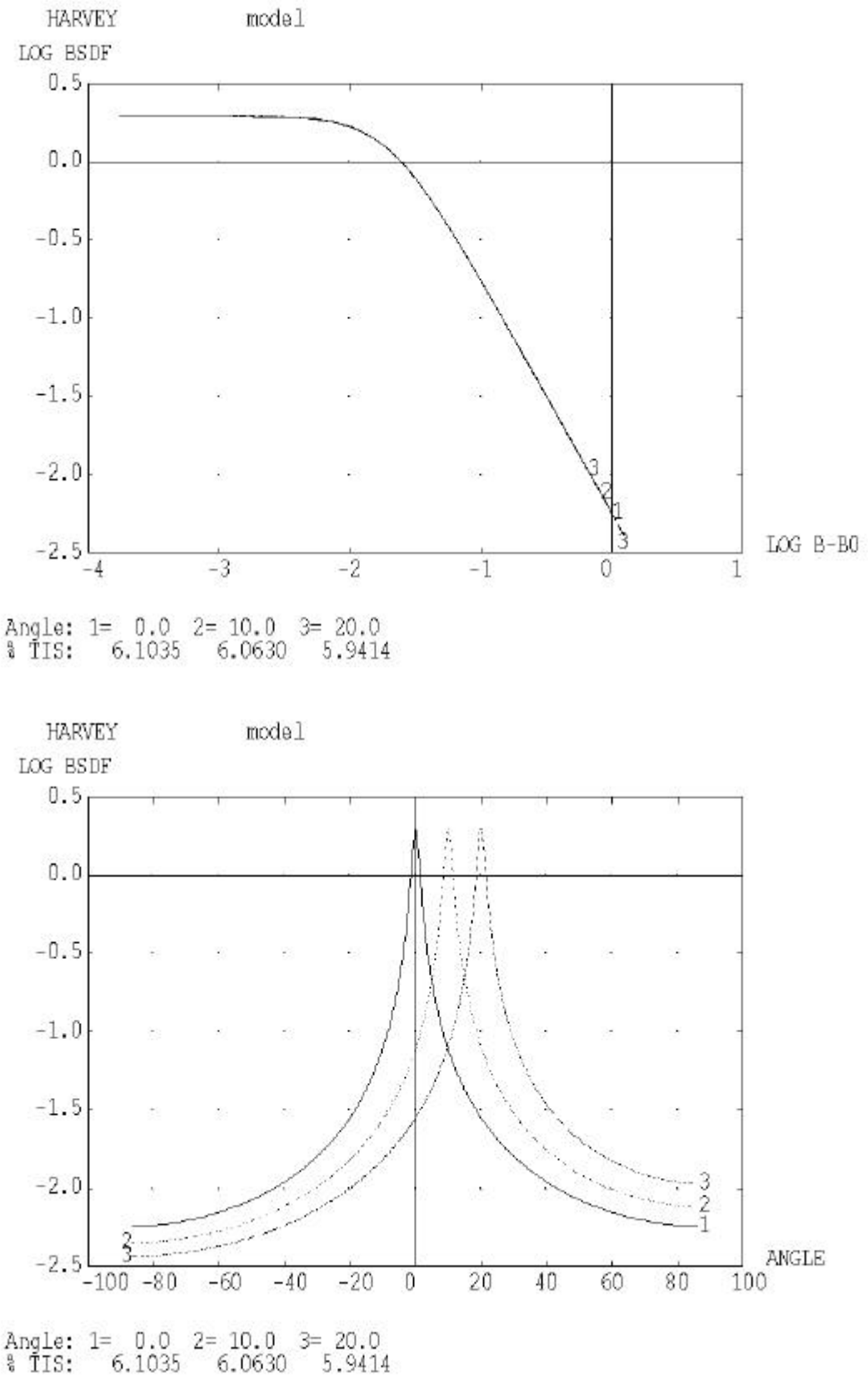

Fig. 5.3-4: Model for SPIRE FP_UNIT, lower part, HARVEY 2 -1.5 0.02
The upper plot mainly shows the values for small scattering angles
The lower plot mainly shows the values for large scattering angles

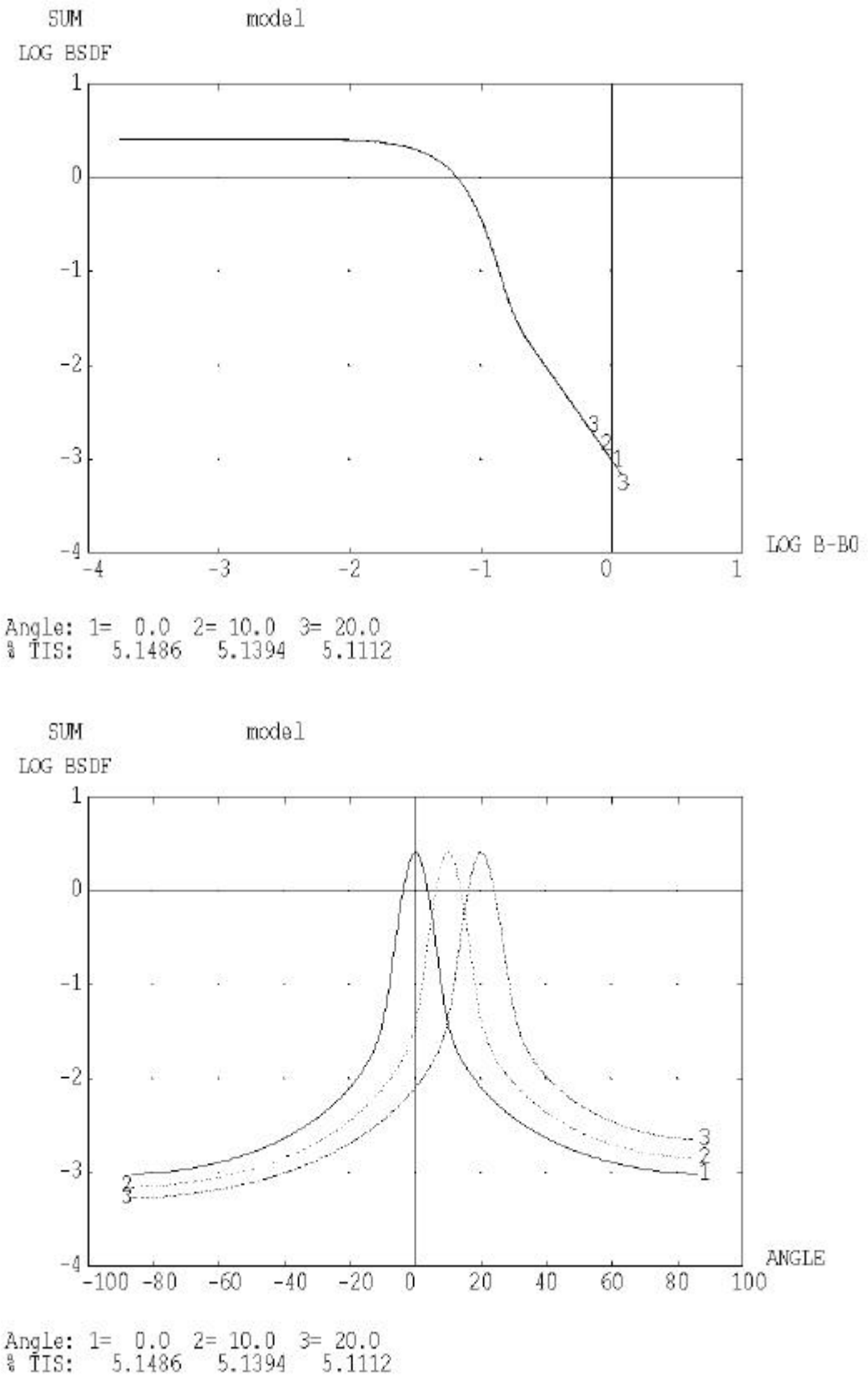

Fig. 5.3-5: Model for SPIRE PFIL1, sum of Harvey 2.0 -50 0.35 and Harvey 0.60 -2.0 0.04
The upper plot mainly shows the values for small scattering angles
The lower plot mainly shows the values for large scattering angles

END OF DOCUMENT

	Name	Dep./Comp.		Name	Dep./Comp.
	Alberti von Mathias Dr.	SM 34		Rühe Wolfgang	ED 6
	Alo Hakan	OTN/IP 35		Runge Axel	OTN/EN 64
	Barlage Bernhard	ED 11		Sachsse Bernt	ED 21
	Bayer Thomas	ED 541		Schäffler Johannes	OTN/EN 64
	Faas Horst	EA 65		Schink Dietmar	ED 422
	Fehringer Alexander	SM 33		Schlosser Christian	OTN/EN 64
	Frey Albrecht	ED 422		Schwabbauer Paul Dr.	OTN/ED 421
	Grasl Andreas	OTN/EN 64		Schweickert Gunn	SM 34
	Grasshoff Brigitte	ED 521		Stauss Oliver	SM 33
	Hartmann Hans Dr.	ED 422		Steininger Eric	ED 422
	Hauser Armin	SM 31		Stritter Rene	ED 11
	Hinger Jürgen	SM 31		Suttner Klaus	SM 32
	Hohn Rüdiger	ED 541		Tenhaeff Dieter	SM 34
	Hölzle Edgar	ED 421		Thörmer Klaus-Horst Dr.	OTN/ED 65
	Huber Johann	ED 543		Wagner Adalbert	OTN/IP 35
	Hund Walter	SE 76		Wagner Klaus	SM 31
	Idler Siegmund	ED 432		Wietbrock, Walter	ED 521
	Ivády von András	ACE 32		Wöhler Hans	SM 34
	Jahn Gerd Dr.	SM 31		Zipf Ludwig	ACE 32
	Kalde Clemens	ED 532			
	Kameter Rudolf	OTN/EN 64			
	Kersting Stefan	OTN/EN 63		Alcatel	ASPI
	Kettner Bernhard	SM 34		ESA/ESTEC	ESA
	Knoblauch August	ED 531			
	Koelle Markus	ED 533		**Instruments:**	
	Kroeker Jürgen	ED 542		MPE (PACS)	MPE
	Kunz Oliver	SM 31		RAL (SPIRE)	RAL
	Lamprecht Ernst	OTN/SM 222		SRON (HIFI)	SRON
	Lang Jürgen	SE 76			
	Langfermann Michael	ED 541		**Subcontractors:**	
	Mack Paul	OTN/EN 64		Air Liquide	AIR
	Maier Hans-Ulrich	ED 11		Astrium Sub-Subsyst. &	ASSE
	Mauch Alfred	SM 34		Austrian Aerospace	AAE
	Moritz Konrad Dr.	ED 65		APCO Technologies S. A.	APCO
	Müller Lutz	OTN/EN 64		Astrium GmbH Space Infrastr.	ASIP
	Muhl Eckhard	OTN/EN 64		BOC Edwards	BOCE
	Pastorino Michel	ASPI Resid.		Dutch Space Solar Arrays	DSSA
	Peitzker Helmut	ED 65		EADS CASA ESPACIO	CASA
	Peltz Heinz-Willi	SM 33		Eurocopter	ECDE
	Peters, Gerhard	ED 531		HTS AG Zürich	HTSZ
	Pietroboni Karin	ED 65		Linde	LIND
	Puttlitz Joachim	OTN/EN 64		Patria New Technologies Oy	PANT
	Raupp Helmut	SM 33		Phoenix, Volkmarsen	PHOE
	Rebholz Reinhold	ED 541		Rembe, Brilon	REMB
	Reuß Friedhelm	ED 62		SENER Ingenieria SA	SEN